



Universitetet  
i Stavanger

**FACULTY OF SCIENCE AND TECHNOLOGY**

## **MASTER'S THESIS**

Study programme/specialization: Information Technology - Automation and Signal Processing	Spring semester, 2018  Open/Confidential
Author: Eivind Hovland	 ..... (signature of author)
Instructor: Professor Kjersti Engan  Supervisor(s): Professor Kjersti Engan & Professor Kathinka Dæhli Kurz	
Title of Master's Thesis: Feature extraction for exploring infarcted regions in perfusion CT images of the brain  Norwegian title: Egenskapsuttrekning for utforsking av infarkt-områder i perfusjon CT-bilder av hjernen	
Credits: 30	
Subject headings:  Ischemic Stroke, Image Registration, Local Binary Pattern, Gray Level Co-occurrence Matrix, Wavelets, Chi-squared, Correlation analysis	Pages: 66 + attachments/other: 23 + embedded file  Stavanger, 15 <sup>th</sup> of June 2018





---

University of  
Stavanger

# Feature extraction for exploring infarcted regions in perfusion CT images of the brain

MASTER'S THESIS

Eivind Hovland

June 2018

Under the supervision of Professor Kjersti Engan  
and Professor Kathinka Dæhli Kurz

Faculty of Technology and Science  
Department of Electrical Engineering and Computer Science  
University of Stavanger

---

---

---

# Abstract

In Norway, over 15 000 people suffer from acute cerebral stroke annually, it is the leading cause of adult long-term severe disability and a significant reason for admission to nursing homes. In Norway it is a prominent cause of death among adults, being the third leading cause of death. On a worldwide basis, 6.7 million deaths were due to stroke in 2012, most of them in low- and medium-income countries.

At Stavanger University Hospital (SUS), patients are routinely investigated using perfusion computed tomography (PCT) in the acute setting. The images acquired are used to calculate parametric color-coded maps describing the blood perfusion in the brain. These maps are interpreted, and thereby aid in deciding whether a patient need immediate thrombolytic treatment. This interpretation is critical in tailoring treatment to each patient, and thus saving lives and reducing the possibility of severe disability. The parametric maps are distant with regards to a certain diagnostic accuracy, and further refinement of the techniques and methods in use are desired. More accurate evaluation of PCT can lead to better guidance of whom to treat with thrombolytic- and interventional therapy, with the goal of better treatment for the patients.

The primary objective of this thesis is to arrange and process the available data material. Additionally, exploration of multiple features that describe a healthy hemisphere of the brain compared to a hemisphere with impaired perfusion is conducted.

Results show that textural features extracted by Local Binary Pattern (LBP) and wavelets can demonstrate a definite difference in the chi-squared distance measured in a healthy hemisphere compared to a hemisphere with impaired perfusion. Over different time-series, the distinctiveness of the features varied, by comparing them to the Time-Density Curves (TDC) for the actual patient, the better features seemed to be extracted from more complex wavelets like Daubechies-4 and Coiflet-4.

Textural features extracted from the Gray Level Co-occurrence Matrices (GLCM) proved challenging to interpret, but by combining them with textural features extracted by Coiflet-wavelets, they were able to distinguish the two hemispheres for each patient.

---

# Preface

This thesis concludes two fantastic years in the city of Stavanger, and at the University of Stavanger.

I would like to thank Professor Kjersti Engan for her invaluable aid, advice and feedback given through the period.

Furthermore, I would like to thank Professor Kathinka Dæhli Kurz for assisting me with medical insight and valuable input concerning the thesis and data material.

Finally, my family and friends, and my partner Martine, deserves my deepest gratitude for supporting me through this period.

Stavanger, 15th of June 2018

*Eivind Hovland*

# Table of Contents

<b>1</b>	<b>Introduction</b>	<b>1</b>
1.1	Image Processing in Medical Applications . . . . .	2
1.2	Thesis objective . . . . .	2
1.3	Thesis outline . . . . .	2
<b>2</b>	<b>Medical Background</b>	<b>5</b>
2.1	Ischemic Stroke . . . . .	5
2.1.1	Infarct Core . . . . .	6
2.1.2	Penumbra . . . . .	6
2.2	Computed Tomography . . . . .	7
2.2.1	Parametric Maps . . . . .	7
2.3	Data Material . . . . .	10
<b>3</b>	<b>Technical Background</b>	<b>13</b>
3.1	Image Registration . . . . .	13
3.2	Histogram Equalization . . . . .	14
3.3	Seeded Region Growing . . . . .	15
3.4	Local Binary Pattern . . . . .	16
3.4.1	Working Principle . . . . .	17
3.4.2	Rotation Invariant . . . . .	17
3.4.3	Uniform Patterns . . . . .	18
3.4.4	Multiresolution Local Binary Pattern . . . . .	19
3.5	Wavelets . . . . .	20
3.6	Gray Level Co-occurrence Matrix . . . . .	21
3.7	Similarity measures . . . . .	23
3.7.1	Chi-Squared distance . . . . .	23
3.7.2	Correlation analysis . . . . .	23
<b>4</b>	<b>Method</b>	<b>25</b>
4.1	Image Registration . . . . .	25

---

4.2	Pre-processing . . . . .	25
4.2.1	Image Normalization . . . . .	25
4.2.2	Histogram Equalizing . . . . .	26
4.3	Masking . . . . .	26
4.3.1	Skull stripping . . . . .	26
4.4	Feature Extraction . . . . .	29
4.4.1	Local binary pattern . . . . .	29
4.4.2	Wavelet . . . . .	30
4.4.3	Model histogram . . . . .	30
4.4.4	Gray Level Co-occurrence Matrix . . . . .	32
4.4.5	Correlation analysis . . . . .	33
4.5	Implementation . . . . .	33
4.5.1	Image registration . . . . .	33
4.5.2	Pre-processing and Masking . . . . .	34
4.5.3	Feature Extraction . . . . .	34
4.5.4	Performance measures . . . . .	34
4.6	Proposed system . . . . .	35
<b>5</b>	<b>Experiments and Results</b>	<b>37</b>
5.1	Masking . . . . .	37
5.2	Experiments . . . . .	37
5.2.1	Experiment 1: Local Binary Pattern . . . . .	38
5.2.2	Experiment 2: Wavelets . . . . .	40
5.2.3	Experiment 3: Gray Level Co-occurrence Matrix . . . . .	41
5.2.4	Experiment 4: Feature selection . . . . .	43
5.2.5	Experiment 5: Correlation analysis . . . . .	45
<b>6</b>	<b>Discussion</b>	<b>47</b>
6.1	Data set . . . . .	47
6.2	Masking . . . . .	47
6.3	Feature Extraction . . . . .	48
6.4	Correlation analysis . . . . .	50
<b>7</b>	<b>Conclusion and Future Work</b>	<b>51</b>
7.1	Future Work . . . . .	51
	<b>Bibliography</b>	<b>53</b>
	<b>Appendices</b>	<b>57</b>

---

---

<b>A</b>	<b>Data material</b>	<b>58</b>
<b>B</b>	<b>MATLAB code</b>	<b>59</b>
<b>C</b>	<b>Features extended: GLCM</b>	<b>60</b>
<b>D</b>	<b>Manually Labeled Penumbra and Infarct Core</b>	<b>63</b>
<b>E</b>	<b>Additional results</b>	<b>64</b>
<b>F</b>	<b>Time-density curve</b>	<b>76</b>

---

# Abbreviations

<b>CBF</b>	Cerebral Blood Flow
<b>CBV</b>	Cerebral Blood Volume
<b>CT</b>	Computed Tomography
<b>CBF</b>	Cerebral Blood Flow
<b>DICOM</b>	Digital Imaging and Communications in Medicine
<b>DWT</b>	Discrete Wavelet Decomposition
<b>GLCM</b>	Gray Level Co-occurrence Matrix
<b>HU</b>	Hounsfield Unites
<b>LBP</b>	Local Binary Pattern
<b>MTT</b>	Mean Transit Time
<b>PCT</b>	Perfusion Computed Tomography
<b>ROI</b>	Region Of Interest
<b>SUS</b>	Stavanger University Hospital
<b>TDC</b>	Time Density Curve
<b>TTP</b>	Time To Peak

# 1 | Introduction

In Norway, over 15 000 people suffer from acute cerebral stroke annually, it is the leading cause of adult long-term severe disability and a significant reason for admission to nursing homes. In Norway it is a prominent cause of death among adults, being the third leading cause of death [1]. On a worldwide basis, 6.7 million deaths were due to stroke in 2012, most of them in low- and medium-income countries [2]. The disease is quite common and has a tremendous negative impact on the quality of life for the patients, and in the acute phase, there is registered mortality of up to 25% [3]. Besides, the costs of healthcare, are colossal for the society [1].

At Stavanger University Hospital (SUS), patients are routinely investigated using perfusion computed tomography (PCT) in the acute setting. The images acquired are used to calculate parametric color-coded maps describing the blood perfusion in the brain. These maps are interpreted, and thereby aid in deciding whether a patient need immediate thrombolytic treatment. This interpretation is critical in tailoring treatment to each patient, and thus saving lives and reducing the possibility of severe disability. The parametric maps are distant with regards to a certain diagnostic accuracy, and further refinement of the techniques and methods in use are desired [4]. More accurate evaluation of PCT can lead to better guidance of whom to treat with thrombolytic- and interventional therapy, with the goal of better treatment for the patients.

Today, PCT provides a good diagnostic accuracy by identifying acute ischemic lesions, but it also has limitations. The limitations appear especially with lesions at pons level and the basal ganglia area. Quantitative analysis has proved to be more efficient [5].

This thesis will focus on feature extraction on PCT images. Local texture analysis will be performed using a data material that consists of 11 patients diagnosed with ischemic stroke. The texture analysis will be conducted using Local Binary Pattern (LBP), Gray-Level Co-occurrence matrix (GLCM) and use of wavelets. The different variations of textural analysis are applied to PCT images that have 4-dimensions (3-D + time).

## 1.1 Image Processing in Medical Applications

Image retrieval within biomedical imaging systems are dependent on digital image processing. Within the field of medicine, image processing techniques have been used both for assisting in diagnosing as well as for research. Image processing applied within the medical field includes morphological image processing, feature extraction and image segmentation [6].

## 1.2 Thesis objective

The primary objective of this thesis is to arrange and process the available data material. Additionally, exploration of multiple features that describe a healthy hemisphere of the brain compared to a hemisphere with impaired perfusion is conducted.

## 1.3 Thesis outline

### **Chapter 2 - Medical Background:**

This chapter presents background theory necessary for the understanding of the thesis. Ischemic stroke, penumbra and the data material are some of the topics outlined.

### **Chapter 3 - Technical Background:**

An overview of relevant theory used throughout the thesis is presented. Among other things are LBP, GLCM and wavelets explained.

### **Chapter 4 - Method:**

An overview of the developed system and its approach is described in detail.

### **Chapter 5 - Experiments and Results:**

Experiments conducted, and results achieved are presented.

### **Chapter 6 - Discussion:**

The chapter presents discussions of data material, concepts and results obtained throughout the thesis.

### **Chapter 7 - Conclusion and Future Work:**

The conclusion of the work conducted is presented. Besides, suggested recommendations for future work are included.

**Appendix A - Data material:**

A time-series of PCT images for patient 1 is presented. The presentation is meant as a helping hand in understanding the structure of the 4-D data material.

**Appendix B - MATLAB Code:**

A list of devised and developed functions are presented. All code described are found in the embedded file, *matlab.7z*.

**Appendix C - Features extended: GLCM:**

From the GLCMs there are extracted a total of 22 features. This thesis focuses on 3 of those 22 features, nevertheless all 22 features are plotted in Appendix C, for patient 1.

**Appendix D - Manually Labeled Penumbra and Infarct Core:**

The data material included PCT images with freehand-drawing estimating the size of the infarct core and penumbra. Table D.1 shows the summarized value of infarct core and penumbra for all patients, measured in  $\text{cm}^2$ . The mean value per slice in the volume is also allocated in table D.1.

**Appendix E - Additional results:**

Chapter 5 mainly presents results from experiments with data material from one patient. In this appendix, results for all patients can be studied closer.

**Appendix F - Time-Density Curves:**

Time-Density curves, as explained in , for all patients, excluding patient 5 can be studied in this appendix.



## 2 | Medical Background

This chapter presents background information within the field of medicine. Ischemic stroke, the acquisition of PCT images and the data material are among topics presented.

### 2.1 Ischemic Stroke

An ischemic cerebral stroke is a result of a transient or permanent reduction in the cerebral blood flow (CBF) to an area of a major brain artery. The reduction in blood flow is caused by an occlusion in the cerebral artery, mainly by an embolus or a local thrombosis [7].

An embolus is a blood clot that breaks free from one part of the circulation system to lodge in another artery, for example, one of the brain arteries. On the other hand, thrombosis is a condition where the blood clot develops in a blood vessel or artery and as a result, reduces the blood flow through this specific vessel or artery. The clot develops as blood changes from a liquid to a solid state, and this produces a mass of coagulated blood [8]. Occlusion of an artery, either in the neck or the brain will deprive parts of the brain of its nutrients, glucose and oxygen [9].

Brain tissue deprived of glucose and oxygen because of compromised blood supply is expected to sustain transient or permanent damage. Brief loss of blood supply can cause cellular changes. Continued loss of blood supply leads directly to death and degeneration of the deprived cells [10]. Figure 2.1, illustrates an ischemic stroke. An occluded artery deprives parts of the brain of its nutrients, seen as the gray area.

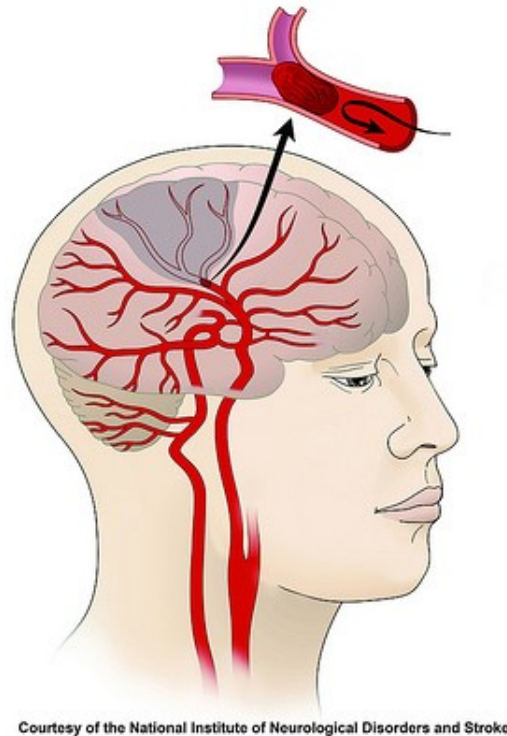


**Figure 2.1:** A visualization of an ischemic stroke in the brain [11]. The gray area is brain tissue deprived of its nutrients, the tissue is in danger of becoming irreversibly damaged. **Reprinted:** National Institute of Neurological Disorders and Stroke, under creative commons(CC), CC-BY-NC 2.0 License.

### 2.1.1 Infarct Core

The infarct core is the part of an ischemic stroke that is already irreversibly damaged. The tissue is not salvageable through reperfusion. In PCT, the infarct core is defined as the area of the brain with increased Time-To-Peak (TTP), markedly decreased CBF and decreased cerebral blood volume (CBV) [12].

### 2.1.2 Penumbra

The penumbra or ischemic penumbra is the part of an acute ischemic stroke that is at risk of progressing to infarction if blood flow is not restored promptly. This part of a stroke is still salvageable. It is usually surrounding the infarct core. The penumbra can be salvaged if it is reperfused fast. When treating a patient with an acute ischemic stroke, the primary objective is to prevent the penumbra from proceeding into an infarct core. By using PCT, the penumbra can be estimated by reviewing parametric maps. The penumbra is described as the area with prolonged T-max, Mean-Transit Time (MTT) or TTP, together with a normal or increased CBV. Unlike the infarct core, the penumbra will only have a moderately decreased CBF [13].

## 2.2 Computed Tomography

Conventional x-rays present three-dimensional objects projected as a two-dimensional image and is a major limitation of conventional radiography. On the other hand, CT overcomes this problem by scanning thin sections of the body with a narrow x-ray beam. The x-ray beam will rotate around the body in a helical shape. The image quality of CT images is typically evaluated using the following criteria:

- Spatial resolution - a description of the ability the system has to define small object distinctly.
- Low-contrast resolution - ability to differentiate objects with similar densities in the image.
- Temporal resolution - describes the speed that the data can be acquired.

Interpretation of CT requires knowledge of anatomy, especially understanding the location of organs relative to other as each CT slice represents a specific plane in the patient's body. The thickness of the acquired slices is defined as the *Z*-axis.

This report focuses on a set of PCT images of the brain. PCT uses a contrast agent to enhance contrast in the tissue. The contrast agent is used in a bolus technique. A CT scan follows a rapid injection of contrast material, images are acquired for the whole volume of the brain through subsequent time intervals. The interval between the injection is initiated and the start time point of the scanning is critical and very important for the result [14]. All patients referred to in this thesis were given 40 ml iodine-containing contrast agent (Omnipaque 350 mg/ml) and 40 ml isotonic saline in a cubital vein with a flow rate of 6 ml/s, the scan delay was four seconds.

### 2.2.1 Parametric Maps

Modern CT scanners have multiple detectors. These can image a substantial volume of tissue both rapidly and repeatedly. The passage of a contrast agent on a series of scans on a specific plane is recorded over time, via a time versus contrast concentration curve [15]. This curve is referred to as a time-density curve (TDC). Using mathematical function of deconvolution on the TDC, various measures of perfusion can be calculated for each image pixel. The measures calculated includes a variety of color-coded parametric maps, these maps are meant to help visualize an acute stroke [16]. A TDC graph can be studied closer in figure 2.2. The *x*-axis on the graph denotes the time elapsed, in seconds, after the start of a bolus injection. The *y*-axis displays the relative enhancement level measured in Hounsfield Units (HU) [14].

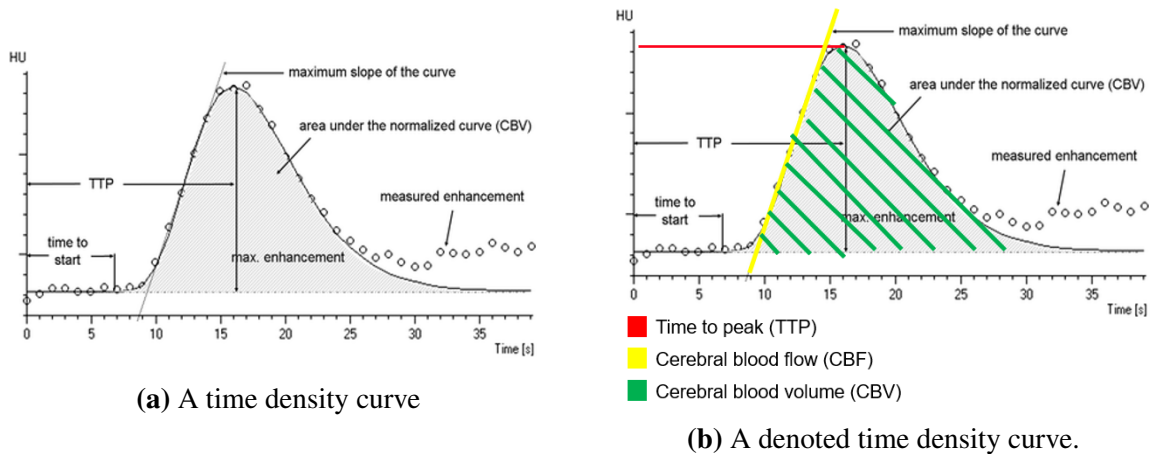


**Figure 2.2:** A denoted time density curve.

The TDCs are generated from images acquired in quick succession. The images are procured at a faster rate in the start, and a decreasing frequency throughout the examination. Examples of typical parametric maps that are generated through deconvolution can be seen in figure 2.3. In addition to these maps, MTT maps are also commonly used. The parametric

### Cerebral blood flow

CBF, as seen in figure 2.3a, is defined as the volume of blood that passes through a given amount of brain tissue per time. It is most commonly measured in milliliters of blood per minute per 100g of brain tissue ( $ml/100g/min$ ) [17].

### Cerebral blood volume

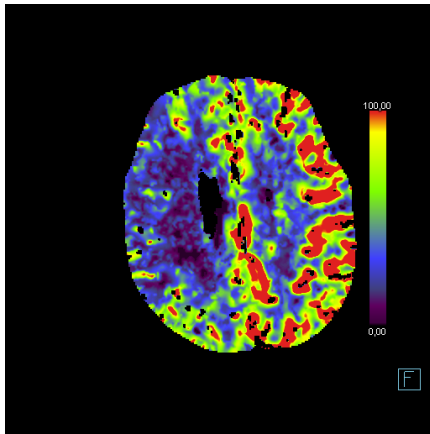
CBV is defined as the volume of blood in a given amount of brain tissue. It is measured as milliliters of blood per 100g of brain tissue ( $ml/100g$ ) [18]. CBV can be calculated by assessing the area under the actual time-density-curve, as seen in figure 2.2b.

### Time-to-peak

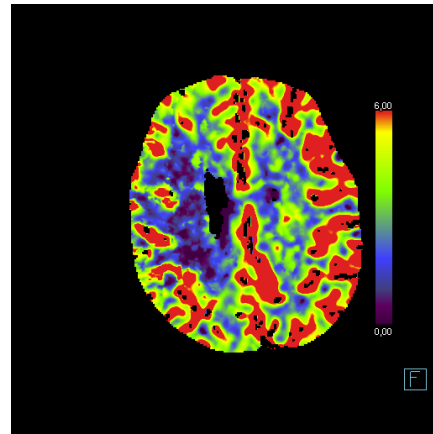
TTP is defined as seen in figure 2.2, it is a measure of the time until the TDC reaches its local maximum. The perfusion map produced by TTP is seen in figure 2.3c.

### T-max

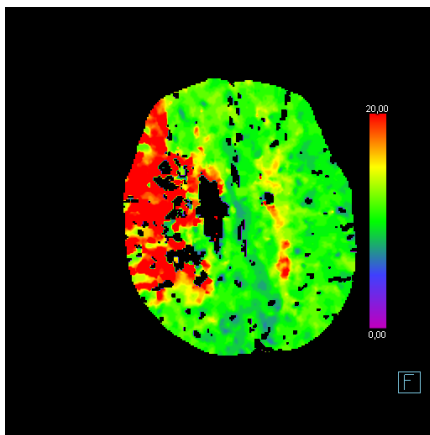
T-max, together with TTP, is a measure of contrast arrival time to the tissue. T-max reflects the time it takes for a contrast agent to reach and traverse areas of the brain, as opposed to the amount of contrast that is measured in a specific point [15]. A parametric color-coded map showing T-max can be studied in figure 2.3d.



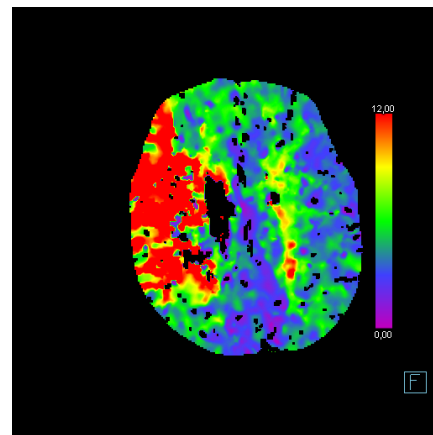
(a) Cerebral blood flow



(b) Cerebral blood volume



(c) Time-to-peak



(d) T-max

**Figure 2.3:** Four different parametric maps frequently used for describing blood perfusion in the brain. The parametric color-coded maps are generated from the TDCs through deconvolution.

## 2.3 Data Material

The data material consists of PCT images of 11 patients obtained at SUS. The images are 4-dimensional (3-D + time). For each patient, there are PCT images as well as parametric colour coded maps which describe the blood perfusion in the brain. Information and comments regarding the patients can be seen in table 2.1.

**Table 2.1:** Overview of information for the 11 patients included in the data material. The table includes information about age, sex, which hemisphere that is perfusion impaired, and if there are any additional comments.

Patient nr.	Age	Sex	Hemisphere affected	Comments
1	64	Male	Right	
2	56	Female	Left	Old infarct - right side
3	67	Female	Right	Old infarct - right side
4	69	Male	Right	Old infarct - right side
5	65	Male	Right	
6	77	Female	Left	Bolus not optimal
7	87	Female	Left	
8	70	Male	Right	
9	63	Female	Left	
10	67	Female	Left	
11	83	Male	Right	

Each patient's PCT examination consists of approximately 30 series, which extend over time, normally 40-50 seconds. For each of these time-series, images are acquired from a volume comprising the central parts of the brain, typically 13 slices. This is visualized in figure 2.4, where  $t_1$  is the first time-series,  $t_{10}$  the tenth time-series,  $t_n$  represents the final time-series. By inspecting the figure closely a difference in the contrast seen in the brain from  $t_1$  to  $t_{10}$  can be regarded, this is a result of the contrast enhancement agent given to the patient.

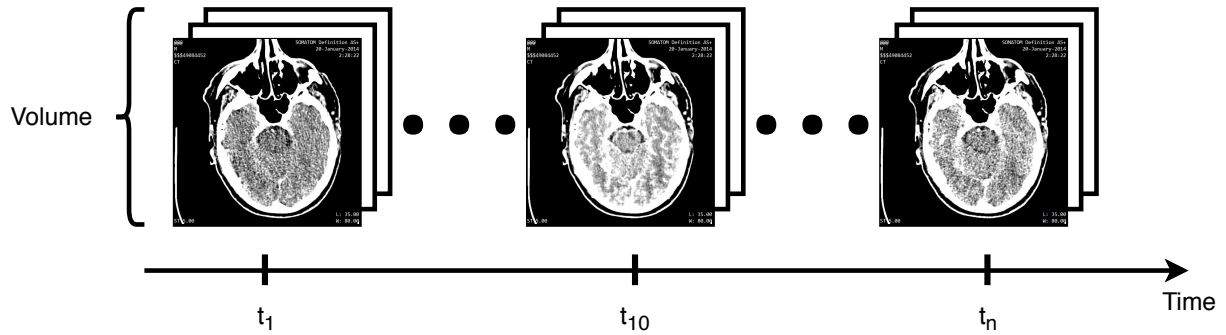


**Figure 2.4:** Visualizing the structure of the 4-D PCT image-series. The volume consists of 13, 15 or 16 images and are repeated for each time-series, typically there are 30 time-series. Consequently, resulting in an image-series consisting of 390, 450 or 480 images.

The data material is in the Digital Imaging and Communications in Medicine (DICOM) standard. The DICOM format contains a header with information about the image as well as patient information [19]. However, it is important to state that the images were anonymized for this study. The images have a resolution of 512 by 512 pixels and the pixels have a bit depth of 16 bits per pixel. The PCT examinations that are the foundation of this thesis consists of 390, 450 or 480 images. That results in respectively 30 time-series of 13, 15 or 16 images per volume-series. A whole volume-series, for patient 1, consisting of 13 slices, can be studied in Appendix A.



## 3 | Technical Background

This chapter presents background information that forms the basis for the research conducted in the thesis. Image normalization, histogram equalization, seeded region growing, Local Binary pattern, wavelets and Gray-level Co-occurrence matrix are presented, in addition, similarity measures used throughout the thesis are described.

### 3.1 Image Registration

Image registration is a fundamental task useful in multiple applications. It is used to coordinate two or more images where the images may have been acquired at different time or viewing points [20]. The data material for this thesis consists of image series where the patient may have moved during an examination.

Kim et al, proposed a robust similarity measure for intramodality image registration in 2004 [21]. Image registration has a goal of finding a geometric transformation, denoted  $T$ , that will align two images  $s_1(\vec{t})$  and  $s_2(\vec{t})$ , where  $\vec{t}$  denotes the spatial coordinates. Image registration based on intensity utilizes a similarity measure based on the image intensity values to achieve its goal. If the transformation,  $T$ , is parameterized using  $\theta^1$ , the case of image registration becomes a parameter estimation problem:

$$\hat{\theta} = \operatorname{argmax}_{\theta} \Phi(s_1(T_{\theta}(\cdot)), s_2(\cdot)) \quad (3.1)$$

In equation 3.1,  $\Phi(s_1, s_2)$  is a measure of the similarity between the images  $s_1$  and  $s_2$ . Registration is in practice performed using a finite samples  $X_i$  and  $Y_i$ , as seen:

$$\begin{aligned} X_i &= s_1(T_{\theta}(\vec{t}_i)) \\ Y_i &= s_2(\vec{t}_i), \quad i = 1, \dots, N \end{aligned} \quad (3.2)$$

In equation 3.2,  $\vec{t}_i$  denotes the sample locations while  $s_1(T_{\theta}(\vec{t}_i))$  is a spatially transformed, and interpolated, version of  $s_1(\vec{t})$ .  $X_i$  depends on  $\theta$ , all quantities computes using  $X_i$  are functions of  $\theta$ .

---

<sup>1</sup>e.g., three translation and three rotation parameters for rigid transformation

$$\hat{\theta} = \operatorname{argmax}_{\theta} \Phi(\mathbf{X}(\theta), \mathbf{Y}) \quad (3.3)$$

where  $\mathbf{X} = (X_1, \dots, X_N)$  and  $\mathbf{Y} = (Y_1, \dots, Y_N)$ . A variety of similarity measures,  $\Phi$ , have been proposed for image registration, among these are statistical quantities including correlation coefficient, as described in [21].

## 3.2 Histogram Equalization

Histogram equalization is a well-known method used in contrast enhancement and standardization of images. Due to its effectiveness, it is widely used in everything from medical image processing to radar image processing [22].

Given an image  $X$ , composed of  $L$  gray levels, the individual luminance levels is described by  $(X_0, X_1, \dots, X_{L-1})$  where  $X(i, j)$  reflects the gray-scale value at the spatial location  $(i, j)$ . For the image, a probability density function,  $p_x(k)$  is defined as:

$$p_x(k) = \frac{n^k}{n}, \quad 0 \leq k \leq L - 1 \quad (3.4)$$

In equation 3.4,  $n$  is representing the total number of pixels in the original image,  $X$ .  $n^k$  represents the number of pixels of value  $k$ . The number of levels,  $L$ , are described as the bit-depth. Based on 3.4, a cumulative density function is defined as:

$$c_x(x) = \sum_{j=0}^k p(j), \quad 0 \leq k \leq L - 1 \quad (3.5)$$

Histogram equalization maps the input image into its entire dynamic range,  $(x_0, x_{L-1})$ , by utilizing the cumulative density function as a transform function. A transform function,  $f(x)$  is defined as:

$$f(x) = X_0 + (X_{L-1} - X_0)c_x(x) \quad (3.6)$$

The histogram equalized output image,  $Y$ , is expressed as

$$Y = f(X) \quad (3.7)$$

$$= \{f(X(i, j)) | \forall X(i, j) \in X\} \quad (3.8)$$

### 3.3 Seeded Region Growing

In 1994, Rolf Adams and Leanne Bischof presented a method of segmentation which utilizes images where regions in the image are characterized by connected pixels of similar value [23]. The first step of the method is to select a set of seed points. From this seed point, the region grows to adjacent pixels depending on a criterion. This criterion can, for example, be pixel intensity or grayscale texture.

Figure 3.1, illustrates how a seeded region growing with a single initial seed positioned in point (3, 3), and a threshold of 1 in a 5x5 image grow. An 8-connected neighborhood is used to examine adjacent pixels of the seed point.

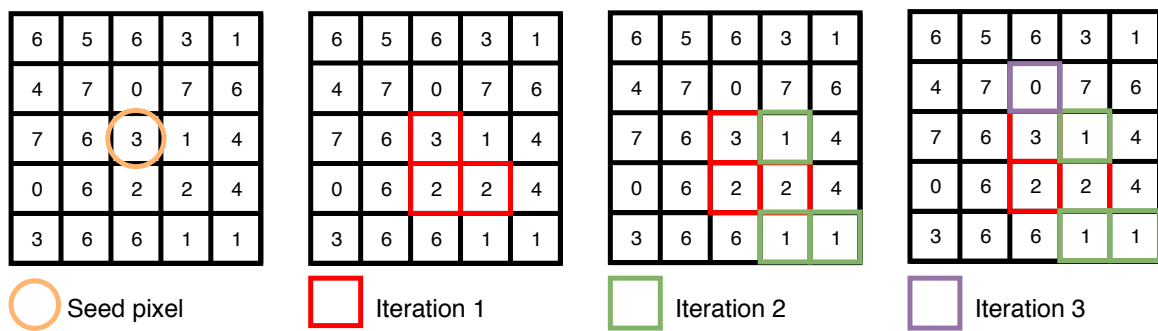


**Figure 3.1:** A 5x5 grayscale image with an initial seed point of (3,3). From the seed point a seeded region grows until all pixels in the region have been allocated with respect to a threshold. This example is conducted using a threshold of 1.

Equation 3.9, is used to determine whether or not the pixel is classified into the seed point. In equation 3.9, the absolute value of the initial seed is subtracted by the adjacent pixels, and compared to a threshold,  $T$ . The process is iterative, and it is repeated until there is no change in two successive iterative stages.

$$|g(\text{seed}) - g(\text{pixel})| \leq T, \quad T = 1 \quad (3.9)$$

Figure 3.2 shows an algorithm scheme of the seeded region growing. The algorithm operates by assigning the pixel coordinate of the initial seed as the starting point of the segmentation procedure, from where the region is expanded, producing a region of interest (ROI) by checking adjacent pixels in the PCT image. The growing criteria, referred to as GC in figure 3.2 is the absolute threshold to be included in the ROI.

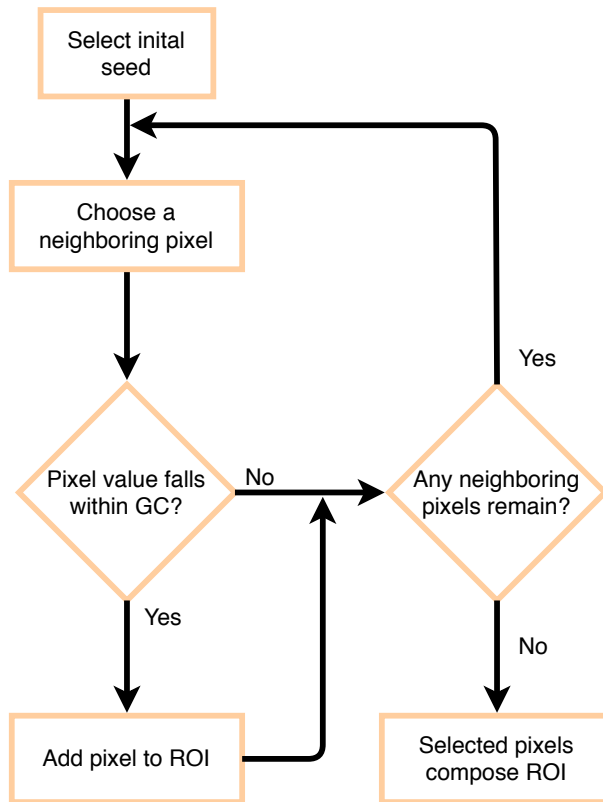


Figure 3.2: Flow-chart of the seeded region growing algorithm.

### 3.4 Local Binary Pattern

In 1996, Ojala et al. introduced a robust way of describing pure LBP in a texture[24]. The algorithm uses a  $3 \times 3$  neighbourhood. For each pixel in the image, a binary label is computed by comparing the center pixel with each of its neighbours, as seen in figure 3.3. The neighborhood is first thresholded by the value of the center pixel before it is multiplied by the weights of the corresponding pixels. Finally, the values of the eight pixels are summed. Hence the number 169 is obtained for this specific texture unit.

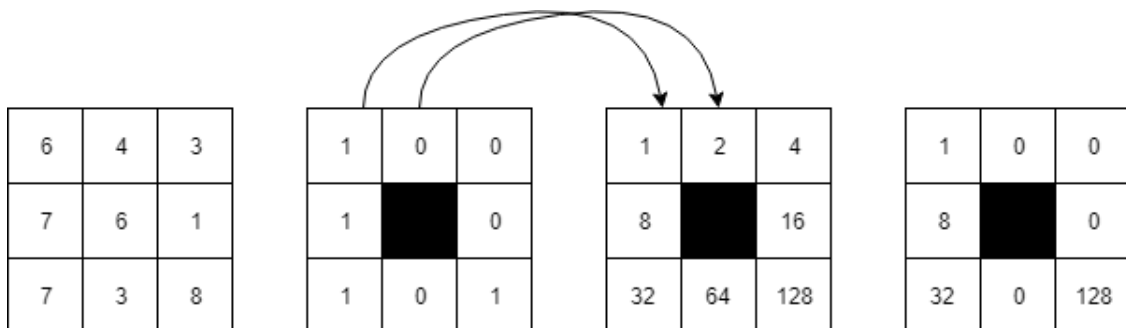


Figure 3.3: A  $3 \times 3$  neighbourhood thresholded by the middle pixel value.

The original LBP operator has limitations. The  $3 \times 3$  neighbourhood does not capture larger

structures in the texture. Ojala et al. therefore extended the operator, so that it could facilitate rotation invariant and uniform pattern analysis at multiple scales [25].

### 3.4.1 Working Principle

Given a random image pixel the circular neighbourhood can be described with a radius,  $r$ , and a fixed number of samples along the circle, as seen in figure 3.4, in this case, there are eight samples in the neighbourhood. If the coordinates of the center pixel,  $g_c$  are  $(0, 0)$  then the coordinates of  $g_p$  are given by  $(-R \sin(\frac{2\pi P}{P}), R \cos(\frac{2\pi P}{P}))$ . Furthermore, if the neighbours do not fall exactly in the center of a pixel, their value is estimated using interpolation.

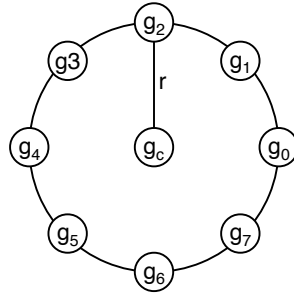


**Figure 3.4:**  $g_c$  is a center pixel surrounded by 8 neighbours. The neighbours are denoted  $g_p$ , in this example  $p$  ranges from 1 to 8.

Each of the labels  $g_p$  are added up to a numeral label through the use of individual weights, as seen in equation 3.10:

$$g_p = 2^p \quad (3.10)$$

The operator, LBP, is denoted with a number of neighbours,  $P$ , and a radius,  $R$  which gives the following definition:

$$LBP_{P,R} = \sum_{p=0}^{P-1} s(g_p - g_c) 2^p \quad (3.11)$$

In 3.11,  $s(x)$  is defined as:

$$s(x) = \begin{cases} 1, & \text{if } x \geq 0 \\ 0, & \text{if } x < 0 \end{cases} \quad (3.12)$$

### 3.4.2 Rotation Invariant

The original LBP operator can be extended by applying rotation invariance [25]. A rotation invariant LBP is preferable as texture rotation tend to be arbitrary.

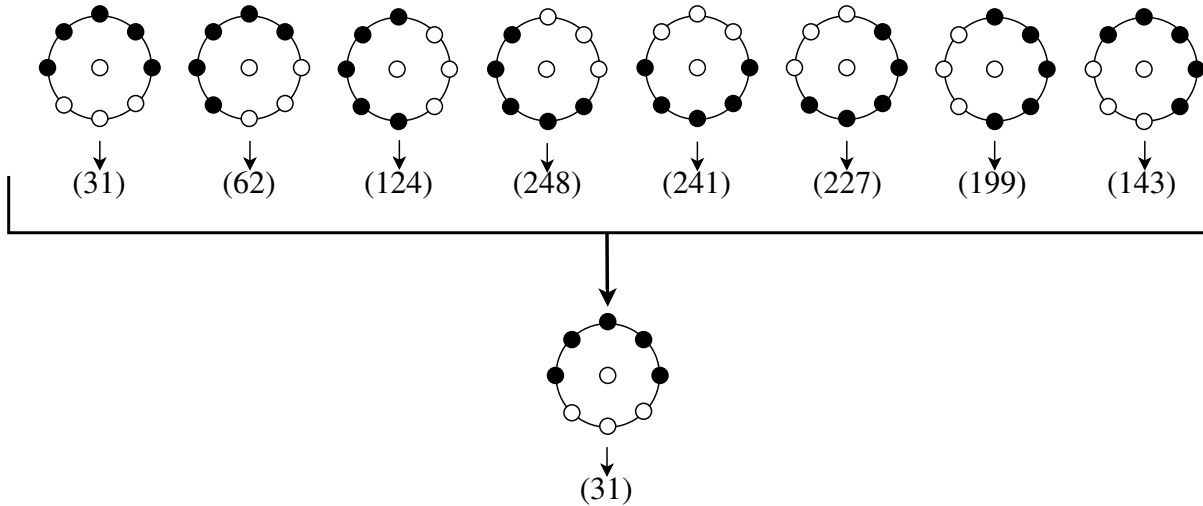


**Figure 3.5:** Illustration of the rotation invariance extension. The minimum possible descriptor is used.

In figure 3.5 black circles are representing ones while white circles are represented as zeroes. The white circles in the middle are considered the center pixel. By applying weights as seen in figure 3.4, eight numeral labels are obtained. The rotation invariant extension uses the minimum possible description through equation 3.13:

$$LBP_{P,R}^{riu^i} = \min\{ROR(LBP_{P,R}, i) \mid i = 0, 1, \dots, P - 1\} \quad (3.13)$$

In 3.13,  $ROR(x, i)$  is a function which performs a circular bit-wise right shift on the  $P$ -bit number  $xi$  times. In figure 3.5, the minimum value found is  $31_{10}$  or  $00011111_2$ , this is assigned as the new label for the center pixel.

### 3.4.3 Uniform Patterns

Another extension of the LBP operator is the use of uniform patterns [25]. The uniform measure is denoted  $U$ , the measure corresponds to the number of spatial transitions in the pattern.

$$LBP_{P,R}^{riu^2} = \begin{cases} \sum_{p=0}^{P-1} s(g_p - g_c), & \text{if } U(LBP_{P,R}) \leq 2 \\ P + 1, & \text{otherwise} \end{cases} \quad (3.14)$$

where

$$U(LBP_{P,R}) = |s(g_{p-1} - g_c) - s(g_0 - g_c)| + \sum_{p=1}^{P-1} |s(g_p - g_c) - s(g_{p-1} - g_c)| \quad (3.15)$$

The superscript  $riu^2$  indicates that the operator in use is invariant to rotations and that it supports uniform pattern, which implies that  $U \leq 2$ . Simplified, the uniformity  $U(LBP_{P,R})$

describes the number of transition between zero and one in the LBP. For example, the following pattern contains two transitions  $11000111_2$  and  $001111000_2$ , while  $01001001_2$  includes five transitions and is therefore not considered uniform.

### 3.4.4 Multiresolution Local Binary Pattern

In [25], a multi-resolution LBP was constructed where it was possible to adjust the radius,  $R$ , and the number of neighbours,  $N$ . Mäenpää and Pietikäinen stated that this method has shortcomings seen from a signal processing view [26]. LBP operators with a large  $R$ , may not result in an adequate representation of two-dimensional images as aliasing effects become an obvious problem. To solve this problem, they introduced an exponentially growing multi-resolution LBP combined with a Gaussian low-pass filter. By applying a low-pass Gaussian filter, the pixel intensity will be collected from a larger area. This will not only remove aliasing but also reduce noise.

With a large radius, the distance between samples becomes large, thereby making the LBP code unreliable. The low-pass filter makes it possible to collect the intensity information for each sample from a larger area, indicated by the solid circles in figure 3.6<sup>2</sup>.

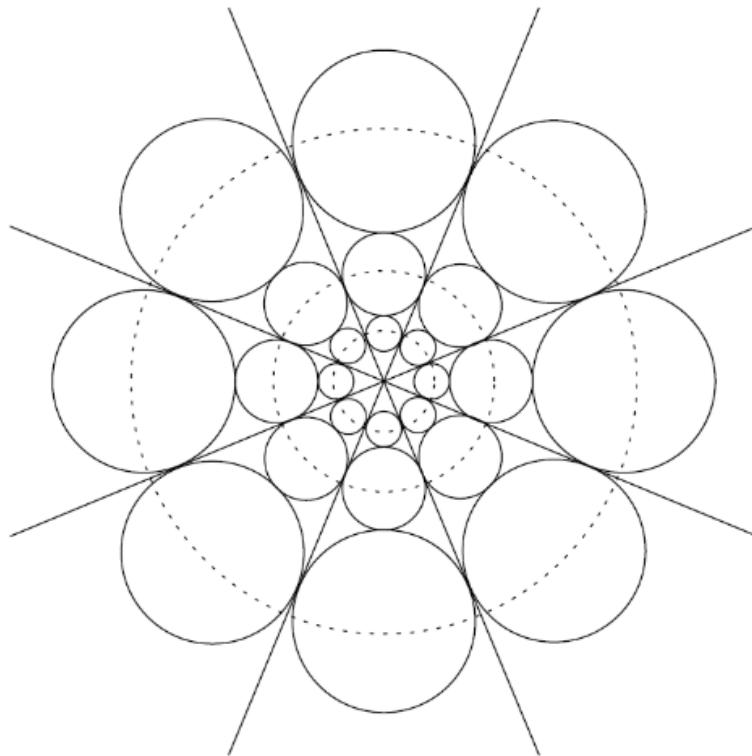


**Figure 3.6:** The effective areas of filtered pixel samples in an eight-bit multi-resolution LBP operator [26].

<sup>2</sup>Reprinted by permission from Springer Nature: Image Analysis 13th Scandinavian Conference, [26] (Multi-scale Binary Patterns for Texture Analysis, Mäenpää and Pietikäinen ),(2003)

The outer radius of this "effective area" with respect to the center of the neighbourhood is described by:

$$r_n = r_{n-1} \left( \frac{2}{1 - \sin\left(\frac{\pi}{P_n}\right)} - 1 \right), \quad n = 2, \dots, N \quad (3.16)$$

In equation 3.16,  $N$  is the number of scales, while  $P_n$  is the number of neighbourhood samples at a scale  $n$ . The use of low-pass filtering is only necessary when the radii is larger than one,  $r_1$  is therefore set to 1.5.  $r_1$  is then the shortest distance between the center and the border of a  $3 \times 3$  neighborhood.

The radii of the LBP operators are chosen so that the effective areas touch each other while they at the same time are non-overlapping. The operator radius,  $R_n$ , at a scale  $n$  ( $N \leq 2$ ) are defined as:

$$R_n = \frac{r_n + r_{n-1}}{2} \quad (3.17)$$

These radii are illustrated by the dotted circles in figure 3.6.

The effective areas are realized using a Gaussian low-pass filter so that 95% of its mass lies within the circle.

## 3.5 Wavelets

Wavelets have in posterity been successfully used in image compression, enhancement, analysis, and classification. It is a mathematical function that can decompose a signal or an image. The decomposition is executed with a series of averaging and difference coefficients [27]. The signals can be represented in different frequency bands by using wavelets, each of the bands will have a resolution matching its scale [28].

The Discrete Wavelet Transform (DWT) of a one-dimensional signal,  $f[n]$ , can be calculated by passing it through a high- and a low-pass filter simultaneously. Assume the low-pass filter has impulse response,  $g[n]$ . The DWT can be evaluated by calculating the convolution of the original signal with the impulse response as:

$$y[n] = (f * g)[n] = \sum_{k=-\infty}^{\infty} f[k] \cdot g[n - k] \quad (3.18)$$

In equation 3.18,  $*$ , indicates the complex conjugate. The wavelet decomposition can be executed using different wavelets, for example, Haar, Daubechies, Symlets, and Coiflets.

For DWT of a two-dimensional image, the original image is convolved along  $x$ - and  $y$ - directions by a low- and high-pass filter. Furthermore, the image is down-sampled by the columns, indicated by  $2 \downarrow$ . The resultant images are the convolved again, this time also with high- and low-pass filters and downsampled again. This process yields four sub-band images, denoted

$LL_1$ ,  $LH_1$ ,  $HL_1$  and  $HH_1$ .  $LL_1$  contains the approximation coefficient and the maximum information of the image, the other sub-band images, in their respective order contains horizontal, vertical and diagonal information about the image, figure 3.7 shows how a 2-D DWT can be applied to an image.

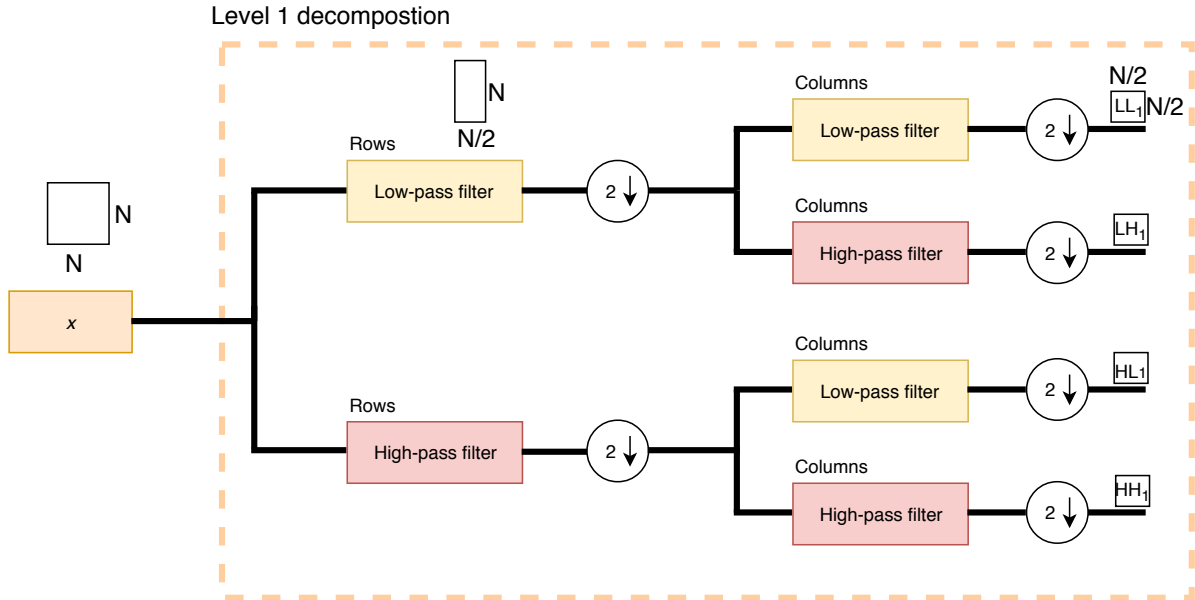


**Figure 3.7:** 1-level sub-band decomposition of an  $N \times N$  image. Suppose an image,  $x$ , of size  $N \times N$ . Each row is low- and high-pass filtered before it is down sampled by the. This results in two  $N \times N/2$  images. Subsequently, the columns are sub-sampled, which gives an output of four images with a resolution of  $N/2 \times N/2$ . The four obtained images can be sub-sampled again, which will give another four new sub-images. This process can be continued until a satisfactory sub-band decomposition is achieved [29].

### 3.6 Gray Level Co-occurrence Matrix

In 1973, Haralick et al. proposed a method for extracting textural features for image classification. They referred to it as Gray-Tone Spatial-Dependence Matrices, today it is most commonly known as Gray Level Co-occurrence matrix (GLCM) [30].

Suppose the image to be analyzed is rectangular with a resolution of  $N_x$  in the horizontal and  $N_y$  in the vertical direction. Each of the gray tone appearing in these cells are then quantized to  $N_g$  levels. Denote  $L_x = \{1, 2, \dots, N_x\}$  as the horizontal spatial domain and  $L_y = \{1, 2, \dots, N_y\}$  as the vertical spatial domain.  $G = \{1, 2, \dots, N_g\}$  is the set of  $N_g$  quantized gray tones. The image,  $I$  can then be represented as a function that assigns a gray tone in  $G$  to each resolution cell or pair of coordinates in  $L_y \times L_x$ ;  $I : L_y \times L_x \rightarrow G$ .

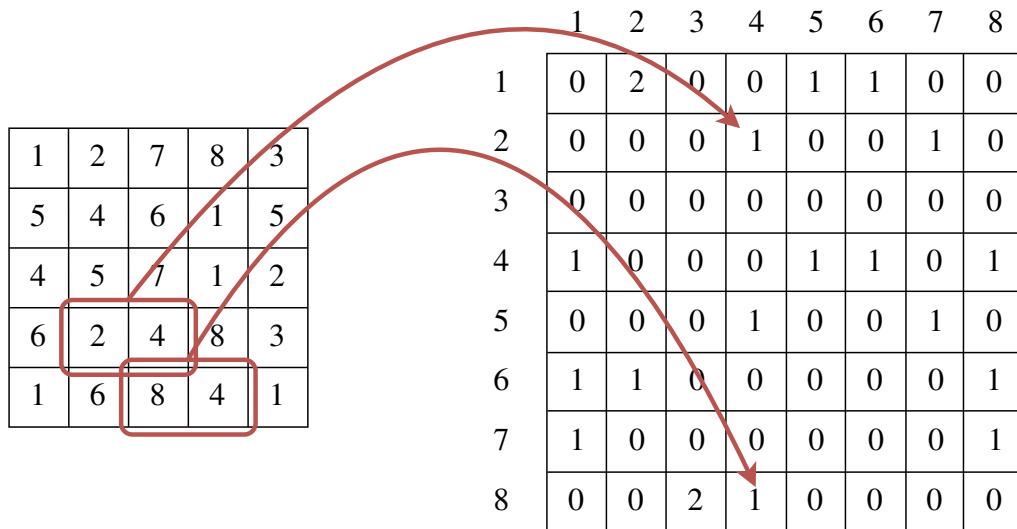


**Figure 3.8:** An illustration of how a  $5 \times 5$  image can be transformed into an  $8 \times 8$  GLCM. The same principle applies for a larger image.

The example in figure 3.8 shows how a  $5 \times 5$  image can be transformed into an  $8 \times 8$  GLCM. The matrix in this example is calculated using the horizontal proximity of the pixels with an offset equal to one. It is possible to explore and test different offsets with various angles. A horizontal offset is considered  $0^\circ$ , while a vertical offset is denoted  $90^\circ$ . Furthermore, it is feasible to use an angle of either  $45^\circ$  or  $135^\circ$ . From the GLCM created, textural features can be extracted. An example of a textural feature extracted is the angular second-moment, which is a measure of homogeneity in the image, see equation 3.19.

$$f_1 = \sum_{i=1}^{N_g} \sum_{j=1}^{N_g} \left( \frac{P(i, j)}{R} \right)^2 \tag{3.19}$$

In equation 3.19,  $P(i, j)$  is the  $i$ th and  $j$ th entry in a GLCM.  $N_g$ , is the number of distinct gray levels in the quantized image while  $R$  is a normalizing constant.

## 3.7 Similarity measures

This section presents methods used for describing differences between a healthy hemisphere of the brain compared to a perfusion impaired hemisphere.

### 3.7.1 Chi-Squared distance

The chi-squared distance, as seen in 3.20, calculates the distance between two histograms where  $x = [x_1, \dots, x_n]$  and  $y = [y_1, \dots, y_n]$  are both having  $n$  bins each.  $d$  is the distance measured between the two histograms.

$$d(x, y) = \frac{1}{2} \sum_{i=1}^{\infty} \frac{(x_i - y_i)^2}{x_i + y_i} \quad (3.20)$$

The chi-squared distance is derived from Pearson's Chi-Squared test which was investigated by Karl Pearson in 1900 [31].

### 3.7.2 Correlation analysis

The correlation coefficient is a measure of linear dependence of two random variables. The Pearson correlation coefficient is defined as [32]:

$$\rho(A, B) = \frac{1}{N-1} \sum_{i=1}^N \left( \frac{A_i - \mu_A}{\sigma_A} \right) \left( \frac{B_i - \mu_B}{\sigma_B} \right) \quad (3.21)$$

where each variable has  $N$  scalar observations.  $\mu_A$  and  $\sigma_A$  are the mean and standard deviation of  $A$ , respectively and  $\mu_B$ , and  $\sigma_B$  are the mean and standard deviation of  $B$ . The correlation coefficient can alternatively be defined in terms of the covariance of  $A$  and  $B$ :

$$\rho(A, B) = \frac{\text{cov}(A, B)}{\sigma_A \sigma_B} \quad (3.22)$$

A correlation coefficient matrix calculated for two random variables results in a pairwise variable combination results in:

$$R = \begin{bmatrix} \rho(A, A) & \rho(A, B) \\ \rho(B, A) & \rho(B, B) \end{bmatrix} \quad (3.23)$$

$A$  and  $B$  are always directly correlated to themselves, the diagonal entries are therefore equal to 1, as seen:

$$R = \begin{bmatrix} 1 & \rho(A, B) \\ \rho(B, A) & 1 \end{bmatrix} \quad (3.24)$$

In addition to correlation coefficients, the P-value is calculated. The P-value gives the user an alternative to a "reject" or "do not reject" approach. If the P-value is lesser than the significance level, 0.05, the corresponding correlation measured in R is considered significant. Otherwise, if the P-value is larger than 0.05, the significance of the measurement plummets [33].

## 4 | Method

In this chapter, each module of the designed system is presented. The modules described can be studied in figure 4.1.



**Figure 4.1:** Simplified overview of the proposed method.

### 4.1 Image Registration

In the DICOM header, information about instance numbers is accessible. The instance number is a number that identifies every image, by using these numbers, the images can be sorted in the order in which they were acquired. For a time-series consisting of 30 series with 15 images per volume, there will be a total of 450 instance numbers. Once the images are sorted according to these numbers, they are registered and aligned with the use of normalized correlation coefficient, as explained and referred to in section 3.1. This process is repeated 11 times, once for each patient.

### 4.2 Pre-processing

This section describes the various steps of pre-processing applied to the images. Images used in the experiments are mainly PCT images, while the perfusion maps are used as a helping hand in understanding where in the brain there are perfusion limitations.

#### 4.2.1 Image Normalization

The grayscale PCT images are normalized. Image normalization is useful as it expands the grayscale so that the images share a similar range. The normalization is implemented using equation 4.1.

$$I_N = (I - Min) \frac{newMax - newMin}{Max - Min} + newMin \quad (4.1)$$

In 4.1,  $I$  represents an image with  $n$ -dimensional grayscale levels with intensity values in the range  $Min$  to  $Max$ .  $I_N$  represents the normalized image, with intensity values in the range of  $newMax$  to  $newMin$ .

## 4.2.2 Histogram Equalizing

In addition to image normalization, the images are also processed using histogram equalization. Histogram equalizing increases the global contrast by a more expedient distribution of the intensities in the histogram.

## 4.3 Masking

This section describes methods and techniques used in the *Masking* block in figure 4.1. A binary mask is created by a seeded region growing.

### 4.3.1 Skull stripping

Skull stripping allows for whole-brain segmentation. The segmentation method is applied with a desire to remove extracerebral tissues<sup>1</sup> from the images. The tissues can be everything from skull and eyeballs to skin [34]. Removing the skull and artifacts are important as they may affect the features extracted, hence the removal may lead to better and more distinct features [35].

The segmentation in this thesis is mainly done by the use of a seeded region growing. Previously to the segmentation, the images are rotated with a fixed angle for each patient. The rotation is done to bring the images into a better horizontal alignment. Afterward, a seeded region growing is placed with an initial position of  $[250, 250]$ . The region then expands by examining neighboring pixels of the initial seed point. A binary mask is constructed from the concluded seeded region growing. Furthermore, if any holes are enclosed in the binary mask, they are filled.

Since the images are registered with respect to each other, it is sufficient to create 13, 15 or 16 binary masks<sup>2</sup> per patient, as masks can be used over whole time-series. Algorithm 1, gives an overview of the method used for creating masks.

If the seeded region growing does not return a satisfactory binary mask for one, or more of the slices in a volume-series, another approach is used to generate appropriate masks. For some patients, it was appropriate to set some of the masks equal as there is so little geometrical change from one slice to another. If this was not applicable, then algorithm 2 is used.

---

<sup>1</sup>Tissue outside the brain

<sup>2</sup>Depending on the total number of images per volume

---

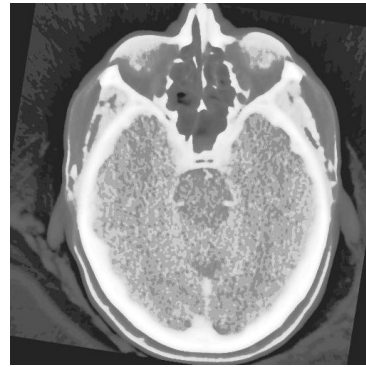
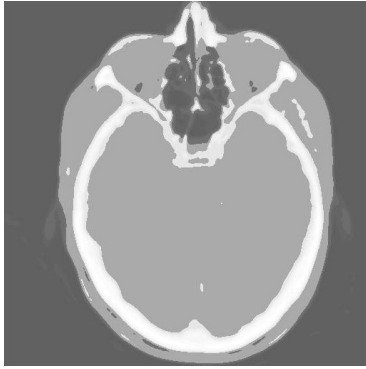
**Algorithm 1:** Preprocessing and skull stripping.

---

```
1 for all images do
2   Sort images with respect to instance number
3   Image registration
4   Rotate with appropriate angle for each patient
5   Normalize 16-bit
6   Histogram equalization
7   for the first volume-series also do
8     Normalize 12-bit
9     Histogram equalization
10    Gaussian low-pass filtering,  $\sigma = 3$ 
11    Seeded region growing, initial seed position [250, 250]
12    Create binary mask from composed ROI
13    Inspect masks
14    if mask successful then
15      | proceed
16    else
17      | Apply algorithm 2 masks
18    end
19  end
20  Apply successful mask
21 end
```

---

By following algorithm 1, it can be interpreted that the first volume-series also are normalized with a lower bit resolution. Moreover, it is filtered by a Gaussian low-pass filter. This approach is applied as it proved that the seeded region growing was better suited for segmenting the brain from the skull. Filtering the image proved to lower the risk of the seeded region growing leaking. Figure 4.2a displays a PCT image pre-processed for mask design by a seeded region growing, while the actual masks constructed were applied to figures pre-processed as the example figure 4.2b show.



(a) A PCT image pre-processed for segmentation. (b) A PCT image pre-processed for feature extraction.

**Figure 4.2:** Two pre-processed image of patient 1, (a) normalized with a 12-bit depth, (b) normalized with a 16-bit depth. Image (a) is better suited for skull-stripping.

---

**Algorithm 2:** Alternative skull stripping.

---

```
1 for image with unsuccessful mask do  
2   | image > threshold  
3   | Remove small objects from the binary image  
4   | Fill image regions and holes  
5 end
```

---

## 4.4 Feature Extraction

This section describes the *Feature Extraction* block in figure 4.1. Ahead of feature extraction, the centroid for each image was calculated. Consequently, for the centroid of the image, the images were split in two. Splitting one image of the brain resulted in two images, one image contained the perfusion impaired hemisphere, while the other half contained the healthy hemisphere. This was carried out for all patients.

### 4.4.1 Local binary pattern

For each of the two hemispheres for each patient, a rotation invariant uniform LBP was computed for every pixel in the image. The images were then masked with the intention of not having the background affect the resulting histograms. The remaining LBP calculated values were added into normalized histograms with  $P+2$  bins, where  $P$  are the number of neighbours. The theory behind the LBP operator is explained in detail in section 3.4. Algorithm 3 presents an overview of the method applied:

---

**Algorithm 3:** Feature extraction of texture information, LBP.

---

```

1 Calculate structure containing mapping table for LBP codes
2 for all masked images do
3     Split images vertically by the centroid
4     for all images with healthy hemispheres do
5         if radius > 1.5 then
6             Apply Gaussian low-pass filter
7             Group data into normalized histograms
8         else
9             Group data into normalized histograms
10        end
11        Calculate the mean of the histograms for each volume-series
12    end
13    for all images with perfusion impaired hemispheres do
14        Repeat line 5-11
15    end
16 end

```

---

Algorithm 3, refers to a mapping table. The mapping table is dependent on whether or not a uniform, rotation invariant or a uniform rotation invariant LBP is applied, by these inputs, it calculates the desired structure. The number of neighbours chosen is also taken into consideration. If radii superior to 1 were chosen, the image was Gaussian low-pass filtered with an appropriate  $\sigma$ , as explained in section 3.4.4.

### 4.4.2 Wavelet

A superficial overview of the applied wavelet method can be seen in algorithm 4.

---

**Algorithm 4:** Feature extraction of texture information, Wavelets.

---

```
1 for all masked images do
2   Split images vertically by the centroid
3   Pad images to make them the same size
4   for all images with healthy hemispheres do
5     Apply two-dimensional DWT
6     Absolute value of coefficients
7     Group data into normalized histograms
8     Calculate the mean for each volume-series
9   end
10  for all images with perfusion impaired hemispheres do
11    Repeat line 5-8
12  end
13 end
```

---

The data material was padded so that all images had the same size. This resulted in a consistent number of coefficients calculated for each image using a discrete wavelet transform. The images of size  $N \times N$  were decomposed using different wavelet transforms. The transforms applied includes the classic Haar-wavelet, Daubechies-4, and Coiflet-4.

Each row was by the respective wavelet filtered and down sampled by the actual filter. This results in two  $N \times N/2$  images. Subsequently, the columns are sub-sampled, which gives an output of four images with a resolution of  $N/2 \times N/2$ . The four obtained images can be sub-sampled again, which will provide another four new sub-images. This process can be continued until a satisfactory sub-band decomposition is achieved [29]. In the experiments conducted a level three sub-band decomposition was used. The absolute value of the coefficients extracted by use of 2-D DWT was calculated for each hemisphere, before grouping them into normalized histograms.

### 4.4.3 Model histogram

A volume-series produced 26, 30 or 32 histograms dependent on the total slices per volume<sup>3</sup>. The histograms were for each hemisphere added together, bin by bin, and divided by the number of slices per volume. This produces a model histogram for the healthy- and the perfusion

---

<sup>3</sup>Two histogram for each time-series, a histogram for the healthy- and a histogram for the perfusion impaired hemisphere.

impaired hemisphere for all patients, resulting in 30 histograms for each prognosis. The process of calculating a model histogram for a time-series is visualized in figure 4.3.

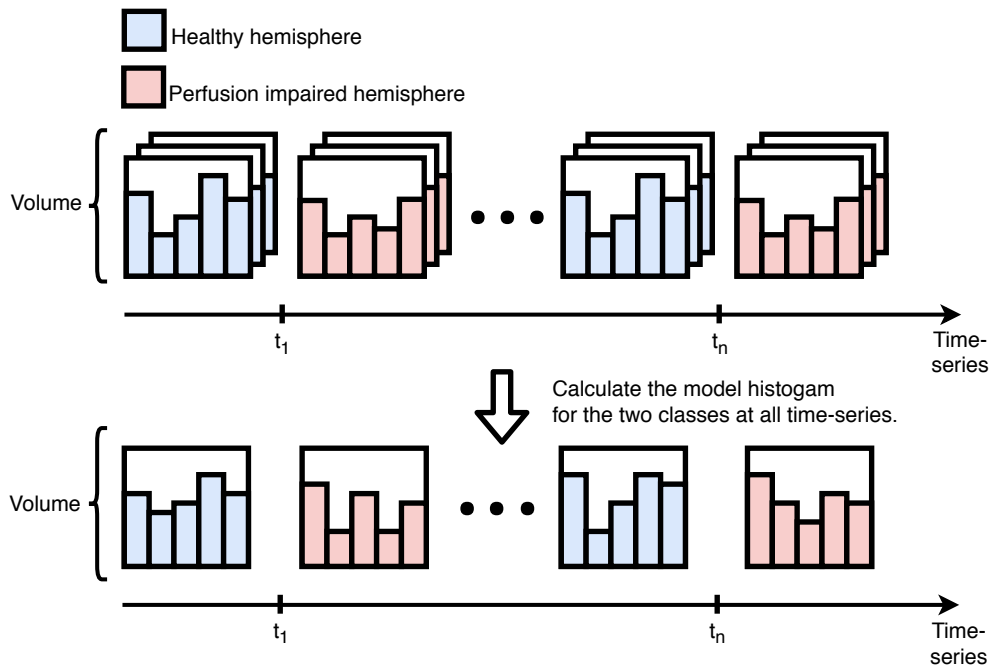


**Figure 4.3:** Visualization of how the model histograms were calculated for a healthy- and a perfusion impaired hemisphere.

Once two model histograms for each time-series was achieved, they were compared by calculating the chi-squared distance using equation 3.20. The chi-squared distance between the healthy hemispheres and the perfusion impaired hemispheres was calculated to indicate if there was possible distinct the two hemispheres over several time-series.

#### 4.4.4 Gray Level Co-occurrence Matrix

A third approach for extracting textural features is through the use of GLCMs. Algorithm 5, gives an overview of the process used.

---

**Algorithm 5:** Feature extraction of texture information, GLCM.

---

```
1 for all masked images do
2   Split images vertically by the centroid
3   for all images with healthy hemispheres do
4     Create gray-level co-occurrence matrices
5     Calculate the mean of each volume-series GLCM
6     Extract textural features
7   end
8   for all images with perfusion impaired hemispheres do
9     Repeat line 4-6
10  end
11  Plot and compare features
12 end
```

---

From the GLCMs it was calculated a total of 22 features, by plotting the features, they were evaluated to identify features that correlated with what was learned from experiments using LBP and wavelets. With that in mind, only a handful of features extracted from the GLCMs are used throughout this thesis. The features that were extracted and studied closer are:

Auto-correlation:

$$f_1 = \sum_i \sum_j (ij)p(i, j) \quad (4.2)$$

Sum of Squares: Variance:

$$f_2 = \sum_i \sum_j (i - \mu)^2 p(i, j) \quad (4.3)$$

where  $\mu$  is the mean value of  $p$ .

Cluster Prominence:

$$f_3 = \sum_i \sum_j (i + j - \mu_x - \mu_y)^4 p(i, j) \quad (4.4)$$

In equations 4.2, 4.3 and 4.4  $p(i, j)$  is the  $(i, j)$ th entry in a normalized GLCM [36]. The mean for the rows and columns of the matrix,  $\mu_x$  and  $\mu_y$  are defined as:

$$\mu_x = \sum_i \sum_j i \cdot p(i, j), \quad \mu_y = \sum_i \sum_j j \cdot p(i, j) \quad (4.5)$$

The features seen in equation 4.2-4.4, were scaled using feature standardization. Standardization of features is used to remove scale effects caused by the use of features with different measurement scales. The equation used for standardization is defined as:

$$x' = \frac{x - \bar{x}}{\sigma} \quad (4.6)$$

In equation 4.6,  $x$  is the original feature vector,  $\bar{x}$  is the mean of the feature vector while  $\sigma$  is its standard deviation [37].

#### 4.4.5 Correlation analysis

The data material also included manually labeled data with freehand-drawings that estimated the area of the penumbra and infarct core for each patient, measured in  $\text{cm}^2$ . This extra data was used to perform a correlation analysis to explore if the chi-squared distances calculated from the LBP and wavelet textural features correlated with the labeled data received. The area under the curve for chi-squared plots were estimated using trapezoidal numerical integration. The chi-squared plots integrated included features extracted using Haar, Daubechies-4 and Coiflet-4 wavelets, additionally,  $\text{LBP}_{16,2-5}^4$ .

The vectors calculated were correlated against information of total penumbra and infarct core size as well as the average value per slice for the two values, the labeled data can be studied in table D.1.

## 4.5 Implementation

Implementation of the proposed system is realized through MATLAB, except image registration which was conducted using ImageJ [38].

### 4.5.1 Image registration

Image registration of the PCT images is achieved by using a plugin for ImageJ; *Template Matching and Slice Alignment*. The plugin includes a function *Align\_slices in Stack*. This function attempt to find a landmark or the most similar image pattern in every slice. The landmark pat-

---

<sup>4</sup>Recall from 3.4.1 the operator, LBP, is denoted with a number of neighbours, P, and a radius, R,  $\text{LBP}_{P,R}$ .

tern will be translated so that it will be in the same position throughout the whole stack. This is used to fix drift of a time-lapse image in stacks [39].

### **4.5.2 Pre-processing and Masking**

Pre-processing the PCT images was done by composing built-in MATLAB functions. The seeded region growing algorithm was realized using a function designed for 2D/3D grayscale images (region\_growing.m<sup>5</sup>, version 1.00) [40].

### **4.5.3 Feature Extraction**

#### **Local Binary pattern**

The LBP operator and its mapping are calculated using implementation available from the University of Oulu (lbp.m, version 0.3.3 and getmapping.m, version 2.0) [41].

#### **Wavelet**

The calculations and implementation of wavelets in this thesis were done through built-in MATLAB functions.

#### **Gray Level Co-Occurrence Matrix**

The GLCMs calculated were done through built-in MATLAB functions. The features extracted from the GLCMs were found using a function that calculates 22 different features from the GLCMs (GLCM\_features1.m<sup>6</sup>) [42].

### **4.5.4 Performance measures**

The chi-squared distance calculated between histograms are calculated using an implementation from Piotr Computer Vision Toolbox (pdist2.m, version 2.0) [43]. The correlation analysis was conducted using built-in MATLAB functions.

---

<sup>5</sup>Copyright (c) 2011, Daniel. All rights reserved.

<sup>6</sup>Copyright (c) 2010, Avinash Uppuluri. All rights reserved.

## 4.6 Proposed system

The proposed system is designed to arrange, process and calculate multiple features describing the PCT images. The system input consists of PCT images for a patient over several volumes- and time-series.

Pay particular attention to how the first volume-series is pre-processed so that it better facilitates a seeded region growing. The successful masks were applied to the images before multiple features were extracted.

The features for a healthy hemisphere of the brain was compared to a perfusion impaired hemisphere for the actual patient calculated by the chi-squared distance. Lastly, the result was evaluated through correlation analysis. A detailed overview of the proposed system can be studied closer in figure 4.4.

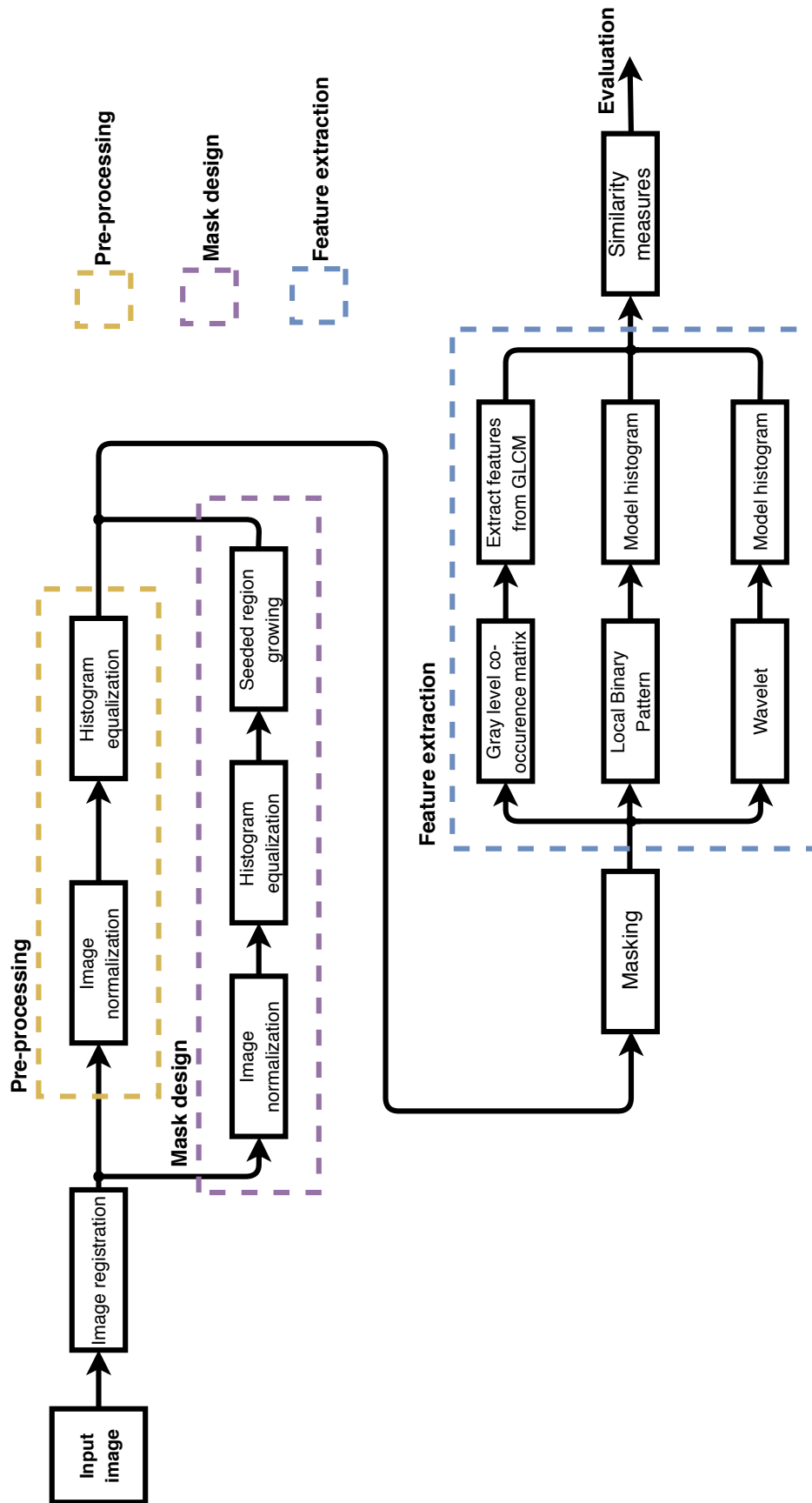


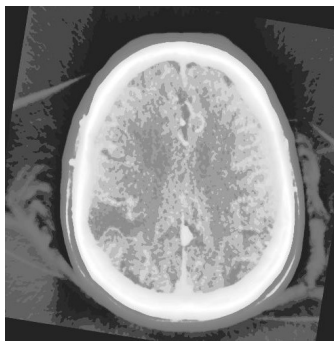
**Figure 4.4:** A detailed overview of the proposed system. Vital parts in the proposed system includes pre-processing, mask design and feature extraction.

## 5 | Experiments and Results

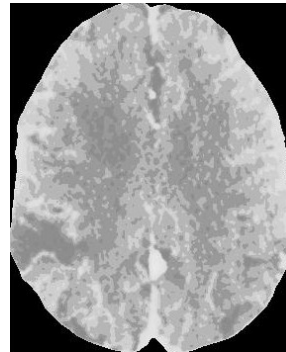
This chapter presents different experiments conducted and results achieved by the use of the proposed method. All results are summarized and discussed in Chapter 6.

### 5.1 Masking

For verification of the generated masks, they were displayed and inspected. If one or more of the masks did not present a satisfactory result, an alternative approach was chosen, as described in section 4.3.1. Figure 5.1 displays a PCT image for patient 3 successfully masked by using a binary mask created from the composed ROI of the seeded region growing.



(a) Before masking.



(b) After masking.

**Figure 5.1:** (a) shows a PCT image for patient 3 before masking. (b) displays the resulting image after a binary mask created from the composed ROI of the seeded region growing is applied to the image.

### 5.2 Experiments

Evaluation of the proposed systems performance was done by calculating the chi-squared distance between features representing a healthy hemisphere compared to a hemisphere with impaired perfusion. Furthermore, the result was compared with software generated TDCs for the actual patients. Features calculated from the GLCMs were compared to the chi-Squared plots generated from LBP and wavelet features, the results were also combined, in a feature selection-like experiment. In addition, a correlation analysis was conducted where results achieved were

correlated with data of the penumbra and infarct core, labelled in  $\text{cm}^2$ .

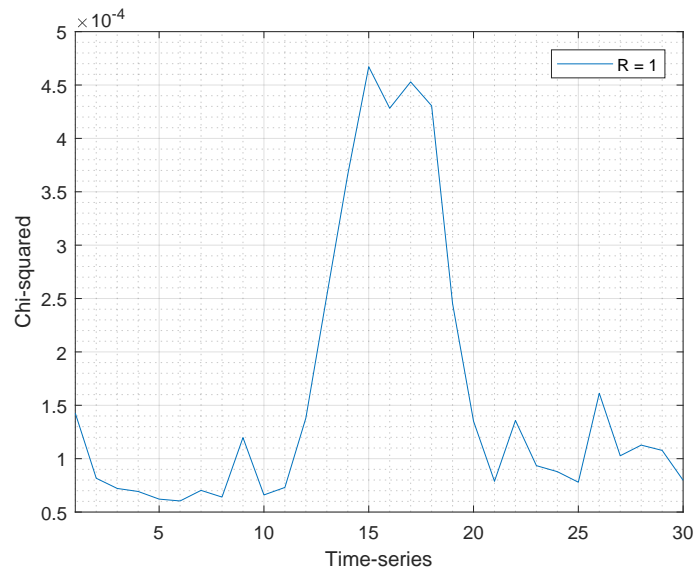
### 5.2.1 Experiment 1: Local Binary Pattern

This experiment was conducted to investigate if a texture feature was able to extract differences in a healthy brain hemisphere with respect to a hemisphere with impaired perfusion. The chi-squared distance was calculated for the features describing the hemispheres. LBP with different parameters were calculated. The different parameters used are visible in table 5.1.

**Table 5.1:** Local Binary Pattern parameters used for textural feature extraction.

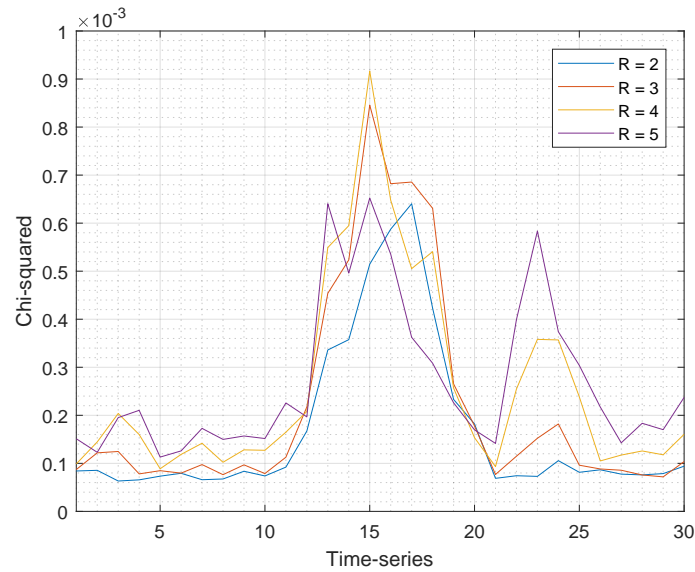
Radius	Neighbours
1	8
2	8, 16
3	8, 16
4	8, 16
5	8, 16

The chi-squared distance for the two hemispheres was calculated for LBP histogram with different radii and neighbours. Figure 5.2, shows the chi-squared distance plotted for patient 1. For this experiment, a radius of 1 and 8 neighbours was used.



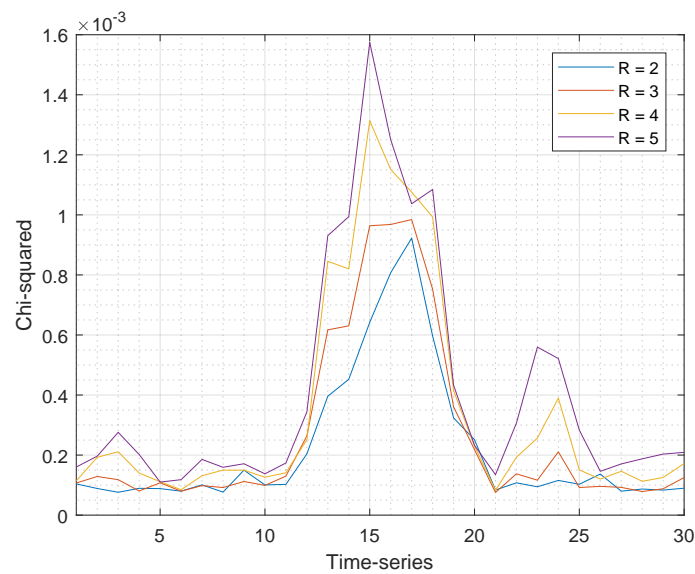
**Figure 5.2:** Chi-squared distance calculated between a healthy- and a perfusion impaired hemisphere. A LBP pattern with 8 neighbours and a radius of 1 was used in this experiment.

Figure 5.3 shows the chi-squared distance plotted for patient 1. This figure contains four graphs. The legend of the plot denotes that four different radii were used, 8 neighbours were used in the calculation.



**Figure 5.3:** Chi-squared distance calculated between a healthy- and a perfusion impaired hemisphere. A LBP pattern with 8 neighbours and a radius ranging from 2-5 was used in this experiment.

Lastly, the LBP descriptor was calculated having 16 neighbours and radii ranging from 2-5. The resulting graphs can be studied in 5.4.



**Figure 5.4:** Chi-squared distance calculated between a healthy- and a perfusion impaired hemisphere for patient 1. An LBP pattern with 16 neighbours and a radius ranging from 2-5 was used in this experiment.

### 5.2.2 Experiment 2: Wavelets

This experiment was devised to identify if texture analysis with wavelets was able to confirm some of the results achieved using LBP. The analysis was based on wavelet decomposition using different wavelet filters and a decomposition level of 3. The experiment was conducted similarly as Experiment 1, where the chi-squared distance was calculated for the features describing the hemispheres.

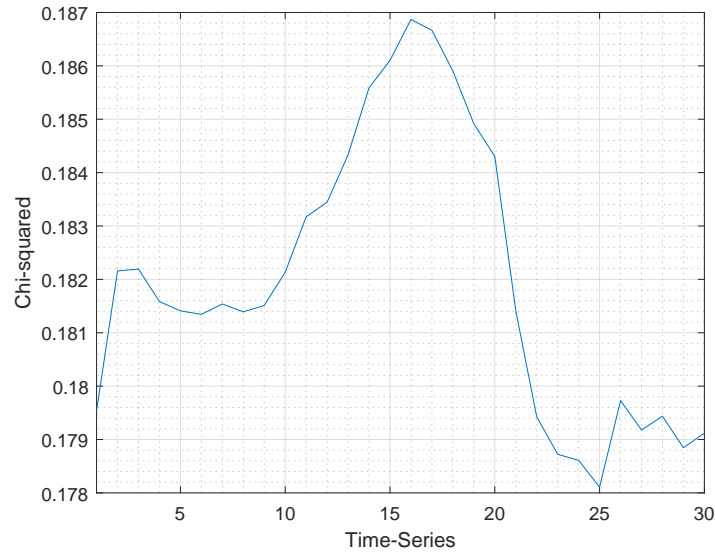


**Figure 5.5:** Chi-squared distance plotted between healthy and perfusion impaired hemisphere for patient 1. Features are extracted by a Haar wavelet, at a level 3 sub-band decomposition.

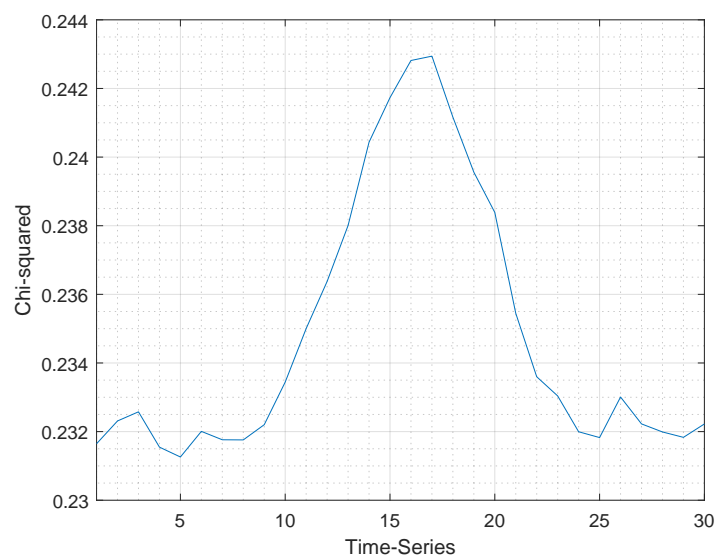


**Figure 5.6:** Chi-squared distance plotted between healthy and perfusion impaired hemisphere for patient 1. Features are extracted by a Daubechies-4 wavelet, at a level 3 sub-band decomposition.

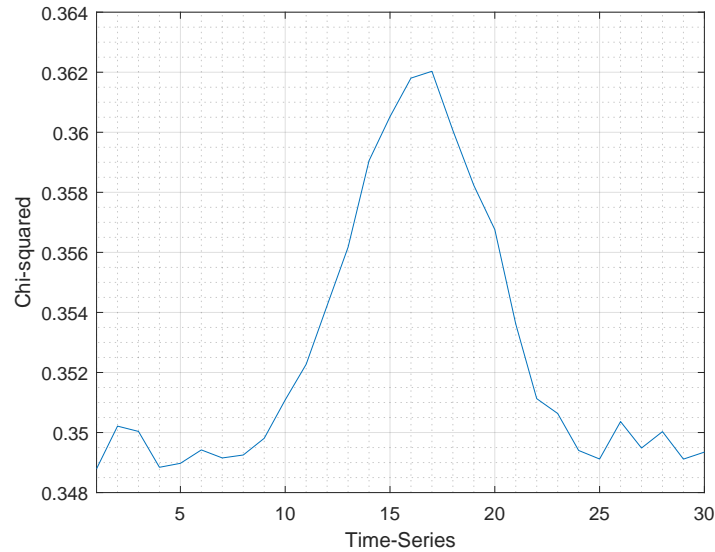


**Figure 5.7:** Chi-squared distance plotted between healthy and perfusion impaired hemisphere for patient 1. Features are extracted by a Coiflet-4 wavelet, at a level 3 sub-band decomposition.

### 5.2.3 Experiment 3: Gray Level Co-occurrence Matrix

Different directions and offsets were calculated and compared. The different directions provided features that were very much alike. Therefore an offset of  $[3, 0]$  is shown throughout this thesis to make an accessible standard of comparison between the patients. In appendix C, all 22 features extracted from the GLCMs with a  $[3, 0]$  offset for patient 1 is shown.

Figure 5.8-5.10 shows textural features extracted from the GLCMs of patient 1. The figures, in their respective order shows auto-correlation, sum-squared: variance and cluster prominence. The features are calculated using equation 4.2-4.4, as described in section 4.4.4. Note the legend in the graphs, this denotes the healthy- and the perfusion impaired hemisphere.

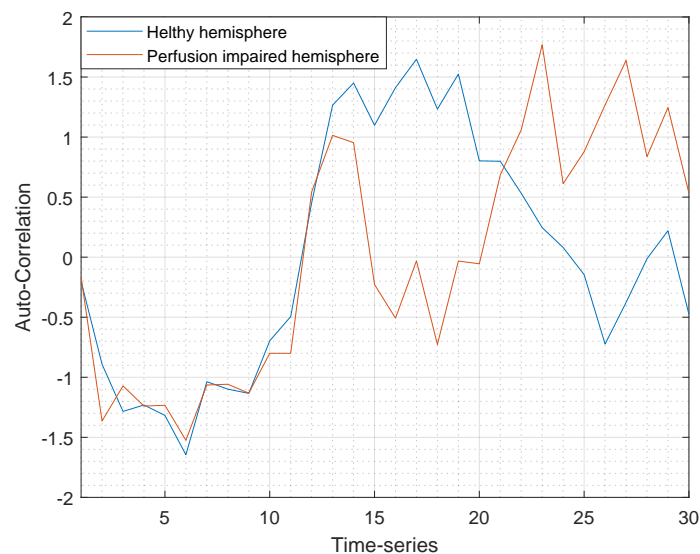


**Figure 5.8:** Auto-correlation feature extracted from patient 1's GLCM.

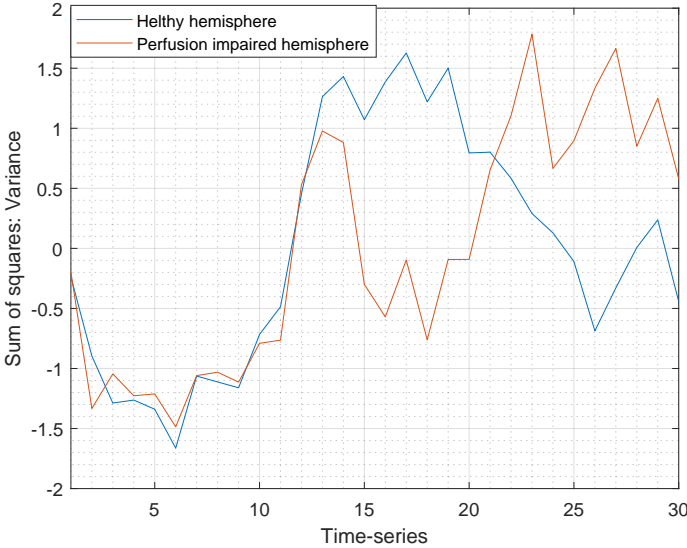


Figure 5.9: Sum of squares: variance feature extracted from patient 1’s GLCM.

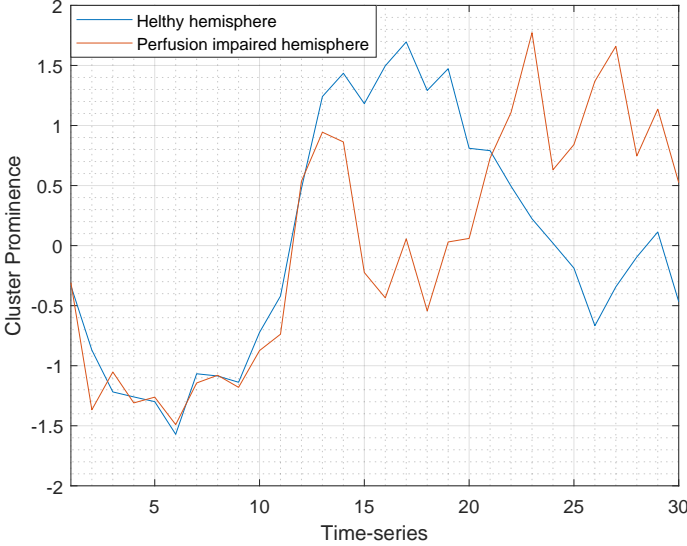


Figure 5.10: Cluster prominence feature extracted from patient 1’s GLCM.

### 5.2.4 Experiment 4: Feature selection

By combining features extracted and plotted, an experiment was conducted to examine if there was possible to decide whether a hemisphere was perfusion impaired or healthy. The experiment was based on a hypothesis that arose from the result seen in figure 5.8, it stated the following: At the local maximum point of either the chi-squared graph for  $LBP_{16,5}$  or Coiflet-4, the healthy hemisphere should have a higher auto-correlation measured compared to the perfusion impaired hemisphere.

Therefore, the local maximum of the chi-squared graphs for  $LBP_{16,5}$  and Coiflet-4 were registered for each patient, and the time-series at this point stored<sup>1</sup>. The time-series number for the local maximums can be studied in table 5.2. The local maximum of the chi-squared graphs describe the time-series that have the most distinctive feature between the two hemispheres.

**Table 5.2:** The time-series(x-value) at the local maximum for the chi-squared distance graphs of  $LBP_{16,5}$  and Coiflet-4 for patients 1-11.

Patient nr.	1	2	3	4	5	6	7	8	9	10	11
Coiflet-4 local maximum	17	18	13	20	16	20	21	18	13	24	20
$LBP_{16,5}$ local maximum	15	23	22	17	13	26	19	15	11	21	26

Figure 5.11 illustrates how the experiment was conducted on patient 3. The leftmost graph is the chi-squared distance calculated between a healthy- and a perfusion impaired hemisphere with  $LBP_{16,2-5}$ . The rightmost graph is the chi-squared distance plotted for Coiflet-4 wavelet with a decomposition level 3.

<sup>1</sup>x-value of the maximum point of the corresponding graphs.

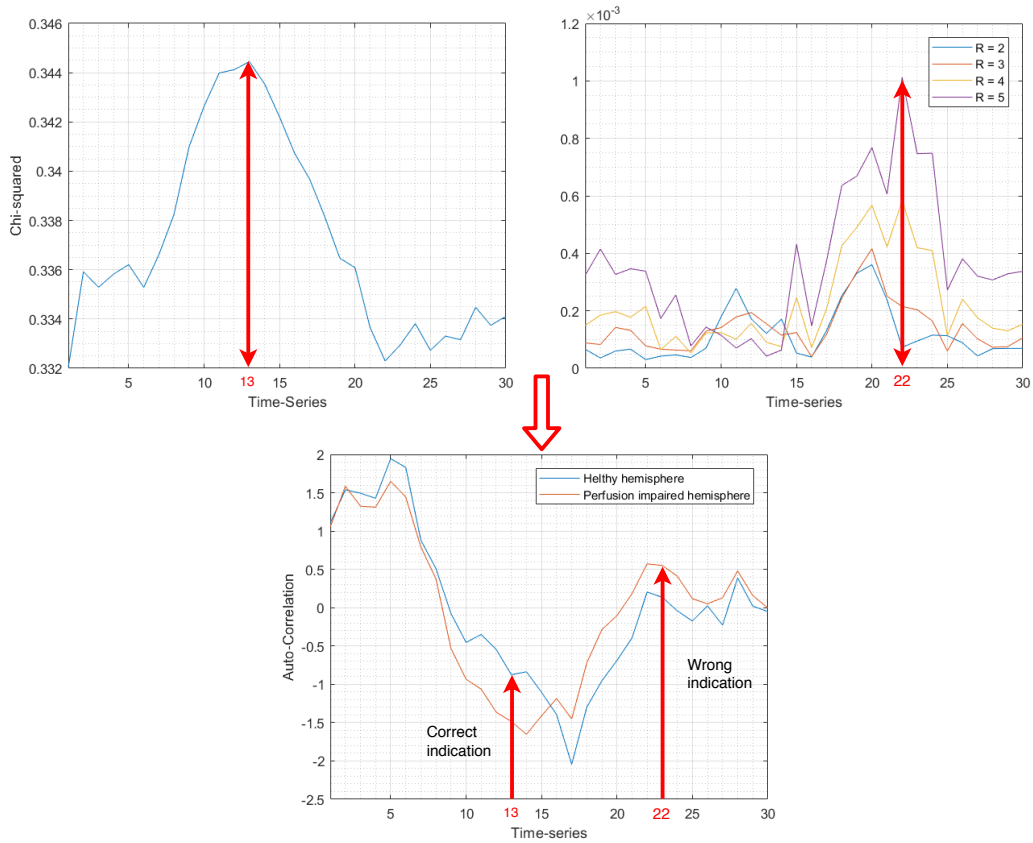


**Figure 5.11:** Illustrating how the most distinctive feature for Coiflet-4 and  $LBP_{16,5}$  was found and used to support the hypothesis.

For figure 5.11, the hypothesis indicated a correct decision using features extracted by utilizing the Coiflet-4 wavelet. On the other hand, features extracted using  $LBP_{16,5}$ , made an incorrect assumption with respect to the propound hypothesis.

This experiment was carried out for all patients, by using data from table 5.2 and combining the with auto-correlation measure extracted from GLCMs. More auto-correlation can be studied closer in E. Experiments using time-series found for Coiflet-4 wavelet resulted in compliances with the hypothesis for 11 out of 11 patients, while  $LBP_{16,5}$  proved right for 7 out of 11 patients with respect to the hypothesis.

### 5.2.5 Experiment 5: Correlation analysis

The data material received also included manually labeled data with freehand-drawings that estimated the area of the penumbra and infarct core for each patient, measured in  $\text{cm}^2$ . A correlation analysis was conducted where the manually (freehand-drawings) labeled data was correlated with the chi-squared distance results achieved. The tests were conducted to investigate if the size of the penumbra and infarct core correlated with the area under the chi-squared graphs for extracted features.

The correlation coefficient between the area under the graph for the chi-squared plot of  $\text{LBP}_{16,4}$  and mean size of penumbra and infarct core gave the following result:

$$R = \begin{bmatrix} 1 & 0.148 \\ 0.148 & 1 \end{bmatrix} \quad P = \begin{bmatrix} 1 & 0.665 \\ 0.665 & 1 \end{bmatrix} \quad (5.1)$$

Correlation between  $\text{LBP}_{16,4}$  and maximum size of penumbra and infarct core for each patient:

$$R = \begin{bmatrix} 1 & 0.191 \\ 0.191 & 1 \end{bmatrix} \quad P = \begin{bmatrix} 1 & 0.575 \\ 0.575 & 1 \end{bmatrix} \quad (5.2)$$

Correlation between the area below the curve of the chi-squared distance of LBP and wavelet textural features were also calculated.  $\text{LBP}_{16,2}$ ,  $\text{LBP}_{16,3}$  and  $\text{LBP}_{16,5}$  all proved to have the highest linear dependence with textural features for Haar-wavelet. The features found to have the highest correlation between each other were  $\text{LBP}_{16,4}$  and Daubechies-4, as the result beneath show:

$$R = \begin{bmatrix} 1 & 0.627 \\ 0.627 & 1 \end{bmatrix} \quad P = \begin{bmatrix} 1 & 0.0389 \\ 0.0389 & 1 \end{bmatrix} \quad (5.3)$$



# 6 | Discussion

## 6.1 Data set

There were some limitations to the study as a result of shallow data material. PCT data from only 11 patients were available. Due to the limited sized data material, an approach where exploring suitable methods of texture analysis were chosen. In addition to an already limited data set, some of the images were omitted from the experiments due to noise. An example is the 4-D data from patient 2. Four images were removed from the patient’s volume-series over all time-series. This narrowed down the data for the actual patient from 450 to 320 images. The images omitted from the volume-series and its corresponding masks can be studied closer in figure 6.1.

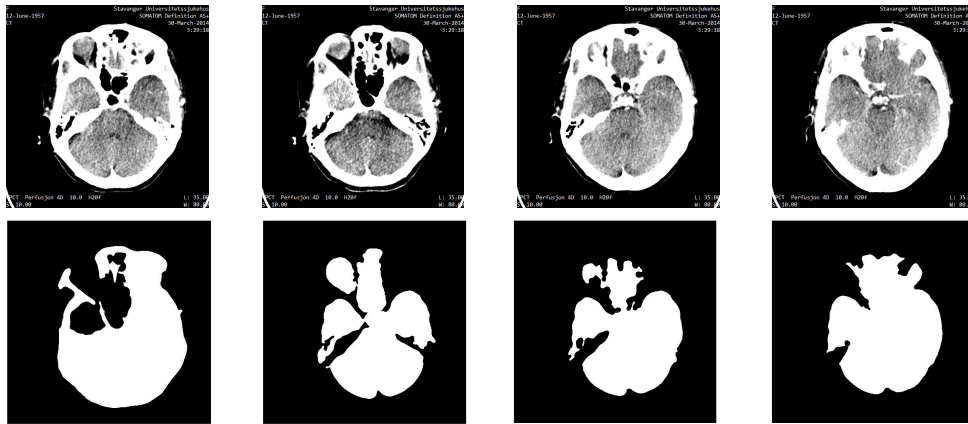


**Figure 6.1:** Images omitted from patient 2’s data set due to noise. The images were omitted so that the noise would not affect the features extracted.

## 6.2 Masking

A drawback in the method used for skull stripping is that there is a chance of the seeded region growing will start leaking if the cranium is not perfectly enclosing the brain, leaking will make the area grow far beyond the region of interest. This issue was attempted resolved by applying a Gaussian low-pass filter to the images used in the mask design. The filter was applied with

the idea that in a smoothed image, there would be a smaller chance of leakage from the region growing. For most images, this solution was satisfactory, while for others, a better solution would be preferable.

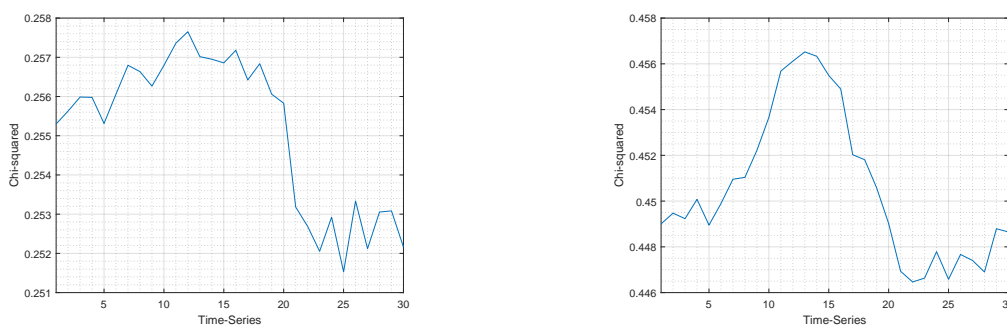
### 6.3 Feature Extraction

#### Experiment 1 & 2

In the implemented system, each image was described by a histogram obtained from LBP descriptor or wavelet coefficients. Histograms for the healthy brain hemispheres were compared to histograms from the hemisphere suffering from impaired perfusion by calculating the chi-squared distance. It is likely that the chi-squared distance calculated was influenced by asymmetry in the brain, but the distance also showed a solid amplification approximately in the middle of the time-series. By comparing the result to the TDCs that are software calculated at the hospital, the textural features extracted using wavelets, and especially Coiflet-4 seemed to have the better resemblance.

A noteworthy observation is that the chi-squared distance for LBP features, or the difference between a healthy- and perfusion impaired hemisphere, was increased by the use of larger radii, more neighbours also increased the distance. It is conceivable that a more significant distance is measured as a radius of 1 will only describe the texture very locally, while larger radii will benefit from information from a larger area.

For features extracted by the use of wavelets, the more complex wavelets seemed to extract more distinct features, with better resemblance to the TDCs. The Haar-wavelet extracted lesser distinct features, and for some patients, this lead to an unclear conclusion. For patient 9, Coiflet-4 extracted distinct features, while the Haar-wavelet seemed to have an uneven distribution of the distinction, see figure 6.2.



(a) Haar-wavelet used for feature-extraction.

(b) Coiflet-4 wavelet used for feature-extraction.

**Figure 6.2:** Distance calculated between the two hemispheres using features extracted respectively by (a) Haar-wavelet and (b) Coiflet-4 wavelet.

### Experiment 3 & 4

The textural features extracted from the GLCMs proved hard to interpret. For some of the patients, the features gave a distinct difference between a healthy- and a perfusion impaired hemisphere of the brain, an example is the auto-correlation feature extracted for patient 1. On the other hand, for other patients, the graphs could almost look arbitrary. The promising result achieved for patient 1, lead to a hypothesis, stated in 5.2.4.

With the hypothesis in mind, an experiment was conducted by using a combination of the features. The time-series having the most distinguishing feature between a healthy- and an impaired hemisphere was located for features extracted from  $LBP_{16,5}$  and Coiflet-4. Furthermore, these specific time-series were studied in auto-correlation feature extracted from the GLCMs. The asserted hypothesis was correct for 11 out of 11 patients using time-series from Coiflet-4 wavelet, while  $LBP_{16,5}$  proved right in 7 out of 11 cases.

There is reason to believe that the Coiflet-4 wavelet outperformed  $LBP_{16,5}$  substantiated in the correlation analysis. The  $LBP_{16,5}$ , when correlated with the textural features extracted by wavelets, proved to have the highest correlation with the Haar-wavelet.

DWT using Haar does not utilize overlapping windows, it only reflects changes between adjacent pixel pairs. The Haar-wavelet uses only two scaling and wavelet function coefficients, thus calculate pairwise averages and differences. Coiflets have a higher computational overhead. In addition, it utilizes overlapping windows. Coiflets, with respect to the Haar-wavelet, have increased capabilities in several image-processing techniques [27].

Another noteworthy pattern in features extracted from the GLCMs is how auto-correlation, cluster prominence and sum of squares: variance all followed their respective patient's TDCs. The TDCs for most plots correlated with regards to which hemisphere that had the highest amplification measured in HU at different time series.

An example is shown here: By taking a closer look at figure 6.3, the following can be seen: LHem (left hemisphere) starts with a higher amplification than RHem (right hemisphere). Afterward, they switch a bit back and forth. At the local maximum, LHem is clearly above RHem, from there on and out, RHem has a higher amplification than LHem. By comparing this to figure 5.8, it can be seen a clear resemblance. This analysis can be carried out for more patients by combining information available in appendix E, which includes results for all patients, and appendix F, which holds TDCs for the patients.

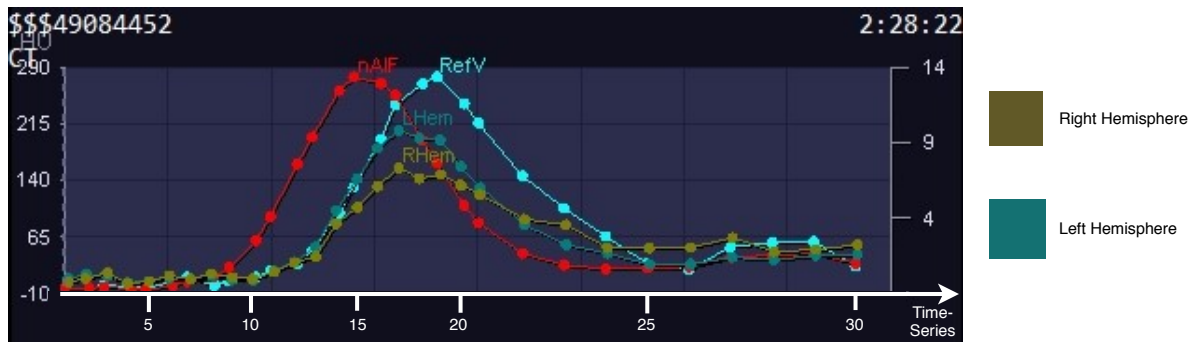


Figure 6.3: TDC for patient 1 with modified x-axis, showing time-series instead of seconds.

## 6.4 Correlation analysis

Correlation between  $LBP_{16,4}$  and the average size of penumbra per slice for the 11 patients scored the highest R-value, 0.148. Although the off-diagonal elements in the matrix of P-values returned a value of 0.665, hence the R-value is classified as non-significant. Moreover, the correlation between the LBP and wavelet features extracted were calculated. The result showed that  $LBP_{16,3}$  and Daubechies-4 had the highest linear dependency, calculated to 0.627, the result is considered significant as the P-value is below 0.05.

The results achieved from the correlation analysis may have been compromised due to a low number of samples. Technically, one can calculate the correlation coefficient having only two samples, although, of little use as the coefficient would always return  $\pm 1$ . In 1938, F.N David recommended that the sample size should be equal or superior to 25 samples [44].

## 7 | Conclusion and Future Work

This thesis elaborates upon a system that explores multiple methods for extracting textural features in PCT images. Images are described by labeled histograms calculated using LBP and wavelets. GLCMs are also calculated for the PCT images, and textural features are extracted from these matrices.

Results show that textural features extracted by LBP and wavelets can demonstrate a definite difference in the chi-squared distance measured in a healthy hemisphere compared to a hemisphere with impaired perfusion. Over different time-series, the distinctiveness of the features varied, by comparing them to the TDCs for the actual patient, the better features seemed to be extracted from more complex wavelets like Daubechies-4 and Coiflet-4.

Textural features extracted from the GLCMs proved challenging to interpret, but by combining them with textural features extracted by Coiflet-wavelets, they were able to distinguish the two hemispheres for each patient.

There is still a lot of work to conduct before a better diagnostic accuracy can be provided for the patients, therefore suggestions for future work are presented in the section below.

### 7.1 Future Work

Future work includes validating results achieved in this thesis on a larger data material. Besides, a more robust method for skull stripping the PCT images would be preferable. Application of different wavelets and the exploration of different decomposition levels for extracting features would also be interesting.

The VAR operator, described in [25] could also be applied, this is likely to show clear differences due to the difference of contrast in the PCT images. With an enlargement of the data material, the features explored in this thesis could be used in a classifying task, a task using labeled tiles of healthy tissue and tissue from the infarct core and penumbra is also a possibility.



# Bibliography

- [1] B Indredavik, R Salvesen, H Næss, and D Thorsvik. Nasjonal retningslinje for behandling og rehabilitering ved hjerneslag. *Oslo: Helsedirektoratet*, page 196, 2010.
- [2] Shanthi Mendis. *Global status report on noncommunicable diseases 2014*. World health organization, 2014.
- [3] Saumya H Mittal, Deepak Goel, et al. Mortality in ischemic stroke score: A predictive score of mortality for acute ischemic stroke. *Brain Circulation*, 3(1):29, 2017.
- [4] YW Lui, ER Tang, AM Allmendinger, and V Spektor. Evaluation of ct perfusion in the setting of cerebral ischemia: patterns and pitfalls. *American Journal of Neuroradiology*, 31(9):1552–1563, 2010.
- [5] Maja Ukmar, Ferruccio Degrassi, Roberta Antea Pozzi Mucelli, Francesca Neri, Fabio Pozzi Mucelli, and Maria Assunta Cova. Perfusion ct in acute stroke: effectiveness of automatically-generated colour maps. *The British journal of radiology*, 90(1072):20150472, 2017.
- [6] Asma Yasrib and Mohd Adam Suhaimi. Image processing in medical applications. 04 2018.
- [7] Werner Hacke, Markku Kaste, Cesare Fieschi, Rüdiger von Kummer, Antoni Davalos, Dieter Meier, Vincent Larrue, Erich Bluhmki, Stephen Davis, Geoffrey Donnan, et al. Randomised double-blind placebo-controlled trial of thrombolytic therapy with intravenous alteplase in acute ischaemic stroke (ecass ii). *The Lancet*, 352(9136):1245–1251, 1998.
- [8] *Concise Medical Dictionary (8 ed.)*. Oxford University Press, 2010.
- [9] Marilyn M. Rymer and Isaac E. Silverman. *Chapter 1 - Stroke Basics*. Clinical Publishing, An Imprint of Atlas Medical Publishing Ltd, Oxford, 2009. Copyright - Copyright Clinical Publishing, An Imprint of Atlas Medical Publishing Ltd. 2009; Last updated - 2010-07-17.
- [10] *Neuroscience*. Sinauer Associates, Sunderland, Mass, 2nd ed. edition, 2001.

- 
- [11] National Institutes of Health et al. Stroke: Challenges, progress, and promise. *Retrieved from this source May*, 5:2011, 2009.
- [12] A.Prof Frank Gaillard et al. Infarct core. <https://radiopaedia.org/articles/infarct-core>. Accessed: 2018-03-10.
- [13] A.Prof Frank Gaillard et al. Ischaemic penumbra. <https://radiopaedia.org/articles/ischaemic-penumbra>. Accessed: 2018-03-10.
- [14] L.E. Romans. *Computed Tomography for Technologists: A Comprehensive Text*. Number poeng 1. Wolters Kluwer Health/Lippincott Williams & Wilkins, 2011.
- [15] Andrew Bivard, Neil Spratt, Christopher R Levi, and Mark W Parsons. Acute stroke thrombolysis: time to dispense with the clock and move to tissue-based decision making? *Expert review of cardiovascular therapy*, 9(4):451–461, 2011.
- [16] Tomasz Hachaj and Marek R Ogiela. Cad system for automatic analysis of ct perfusion maps. *Opto-Electronics Review*, 19(1):95–103, 2011.
- [17] Dr Dan J Bell and A.Prof Frank Gaillard et al. Cerebral blood flow (cbf). <https://radiopaedia.org/articles/cerebral-blood-flow-cbf>. Accessed: 2018-03-11.
- [18] Dr Dan J Bell and A.Prof Frank Gaillard et al. Cerebral blood volume (cbv). <https://radiopaedia.org/articles/cerebral-blood-volume-cbv>. Accessed: 2018-03-11.
- [19] Peter Mildenerger, Marco Eichelberg, and Eric Martin. Introduction to the dicom standard. *European Radiology*, 12(4):920–927, Apr 2002.
- [20] Lisa G Brown. A survey of image registration techniques, 1991.
- [21] Jeongtae Kim and Jeffrey A Fessler. Intensity-based image registration using robust correlation coefficients. *IEEE transactions on medical imaging*, 23(11):1430–1444, 2004.
- [22] Yeong-Taeg Kim. Contrast enhancement using brightness preserving bi-histogram equalization. *IEEE transactions on Consumer Electronics*, 43(1):1–8, 1997.
- [23] Rolf Adams and Leanne Bischof. Seeded region growing. *IEEE Transactions on pattern analysis and machine intelligence*, 16(6):641–647, 1994.
- [24] Timo Ojala, Matti Pietikäinen, and David Harwood. A comparative study of texture measures with classification based on featured distributions. *Pattern recognition*, 29(1):51–59, 1996.

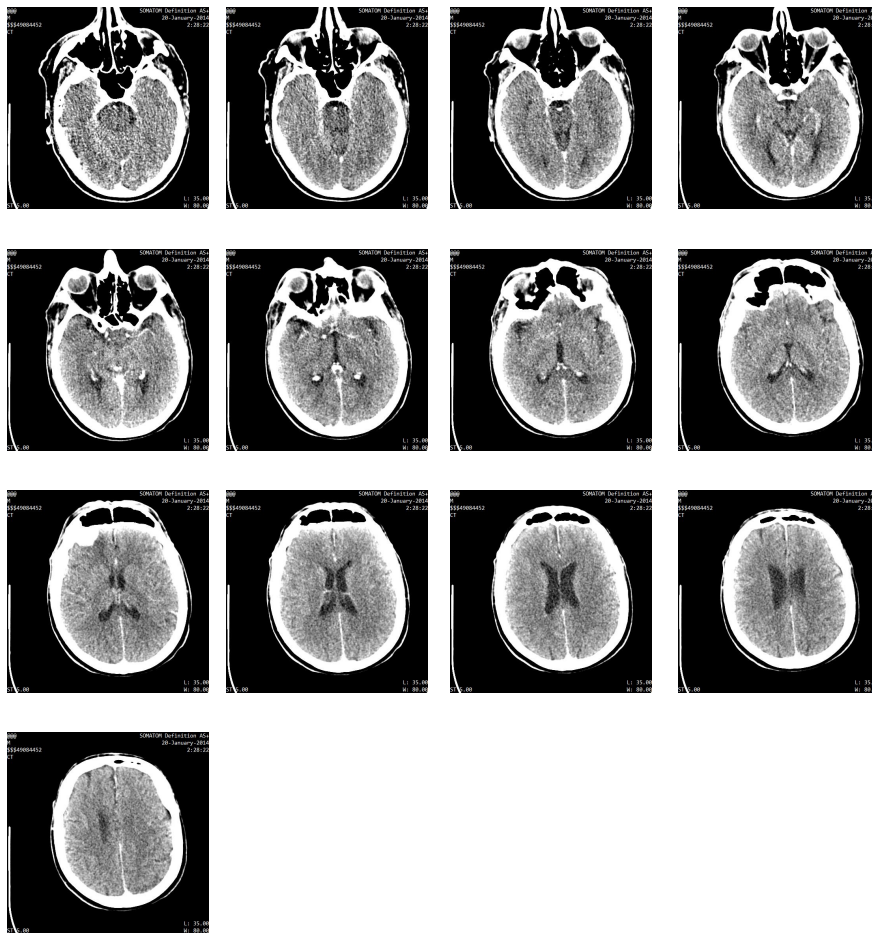
- 
- [25] Timo Ojala, Matti Pietikainen, and Topi Maenpaa. Multiresolution gray-scale and rotation invariant texture classification with local binary patterns. *IEEE Transactions on pattern analysis and machine intelligence*, 24(7):971–987, 2002.
- [26] Topi Mäenpää and Matti Pietikäinen. Multi-scale binary patterns for texture analysis. In *Scandinavian Conference on Image Analysis*, pages 885–892. Springer, 2003.
- [27] Lindsay Semler, Lucia Dettori, and Jacob Furst. Wavelet-based texture classification of tissues in computed tomography. In *Computer-Based Medical Systems, 2005. Proceedings. 18th IEEE Symposium on*, pages 265–270. IEEE, 2005.
- [28] Agma JM Traina, Cesar AB Castañón, and C Traina. Multiwavemed: a system for medical image retrieval through wavelets transformations. In *Computer-Based Medical Systems, 2003. Proceedings. 16th IEEE Symposium*, pages 150–155. IEEE, 2003.
- [29] Khalid Sayood. Introduction to data compression, 2006.
- [30] Robert M Haralick, Karthikeyan Shanmugam, et al. Textural features for image classification. *IEEE Transactions on systems, man, and cybernetics*, (6):610–621, 1973.
- [31] Karl Pearson. X. on the criterion that a given system of deviations from the probable in the case of a correlated system of variables is such that it can be reasonably supposed to have arisen from random sampling. *The London, Edinburgh, and Dublin Philosophical Magazine and Journal of Science*, 50(302):157–175, 1900.
- [32] Mathworks. Correlation coefficients. <https://se.mathworks.com/help/matlab/ref/corrcoef.html>. [Online; accessed 15-April-2018].
- [33] Ronald E Walpole, Raymond H Myers, Sharon L Myers, and Keying Ye. *Probability and statistics for engineers and scientists*, volume 5. Macmillan New York, 1993.
- [34] Florent Ségonne, Anders M Dale, Evelina Busa, Maureen Glessner, David Salat, Horst K Hahn, and Bruce Fischl. A hybrid approach to the skull stripping problem in mri. *Neuroimage*, 22(3):1060–1075, 2004.
- [35] Sudipta Roy, Sanjay Nag, Indra Kanta Maitra, and Samir Kumar Bandyopadhyay. Artefact removal and skull elimination from mri of brain image. *International Journal of Scientific and Engineering Research*, 4(6):163–170, 2013.
- [36] L-K Soh and Costas Tsatsoulis. Texture analysis of sar sea ice imagery using gray level co-occurrence matrices. *IEEE Transactions on geoscience and remote sensing*, 37(2):780–795, 1999.
- [37] Leif E Peterson. K-nearest neighbor. *Scholarpedia*, 4(2):1883, 2009.
-

- 
- [38] Caroline A Schneider, Wayne S Rasband, and Kevin W Eliceiri. Nih image to imagej: 25 years of image analysis. *Nature methods*, 9(7):671, 2012.
- [39] Qingzong Tseng. Template matching and slice alignment – imagej plugins. <https://sites.google.com/site/qingzongtseng/template-matching-ij-plugin>. Accessed: 2018-02-10.
- [40] Daniel. Region Growing (2D/3D grayscale). <https://ww2.mathworks.cn/matlabcentral/fileexchange/32532-region-growing--2d-3d-grayscale->, 2011. [Online; accessed 20-February-2018].
- [41] University of Oulu. Local binary pattern, MATLAB implementation. <http://www.cse.oulu.fi/CMV/Downloads/LBPMatlab>, 2014. [Online; accessed 2-February-2018].
- [42] Avinash Uppuluri. GLCM\_Features4 - Calculates the texture features from the different GLCMs. <https://se.mathworks.com/matlabcentral/fileexchange/22354-glcm-features4-m--vectorized-version-of-glcm-features1-m--with-code-changes-?focused=5150004&tab=function>, 2010. [Online; accessed 20-February-2018].
- [43] Piotr Dollár. Piotr’s Computer Vision Matlab Toolbox (PMT). <https://github.com/pdollar/toolbox>.
- [44] Douglas G Bonett and Thomas A Wright. Sample size requirements for estimating pearson, kendall and spearman correlations. *Psychometrika*, 65(1):23–28, 2000.
- [45] David A Clausi. An analysis of co-occurrence texture statistics as a function of grey level quantization. *Canadian Journal of remote sensing*, 28(1):45–62, 2002.

# Appendices

# A | Data material

The 13 images seen below represents the first volume-series captured for patient 1. For a PCT examination, 30 of these volume-series are acquired over time, making the data material consisting of 4-dimensions.



## B | MATLAB code

The following MATLAB files are embedded in *matlab.7z*.

### **calculate\_glcm.m**

Calculates GLCMs from the input images.

### **correlation\_analysis.m**

Computes the results achieved in experiment 5, correlation analysis.

### **extract\_lbp\_features.m**

LBP descriptor is calculated for several images.

### **extract\_wavelet\_features.m**

Wavelet features are extracted from the images.

### **getmapping.m**

Computes the mapping required for lbp.m [41].

### **GLCM\_Features1.m**

Calculates 22 different features from input GLCM(s) [42].

### **img\_norm.m**

Image normalization.

### **lbp.m**

Computes the LBP descriptor [41].

### **pdist2.m**

Calculates the chi-squared distance between histograms [43].

### **pre\_processing\_masking.m**

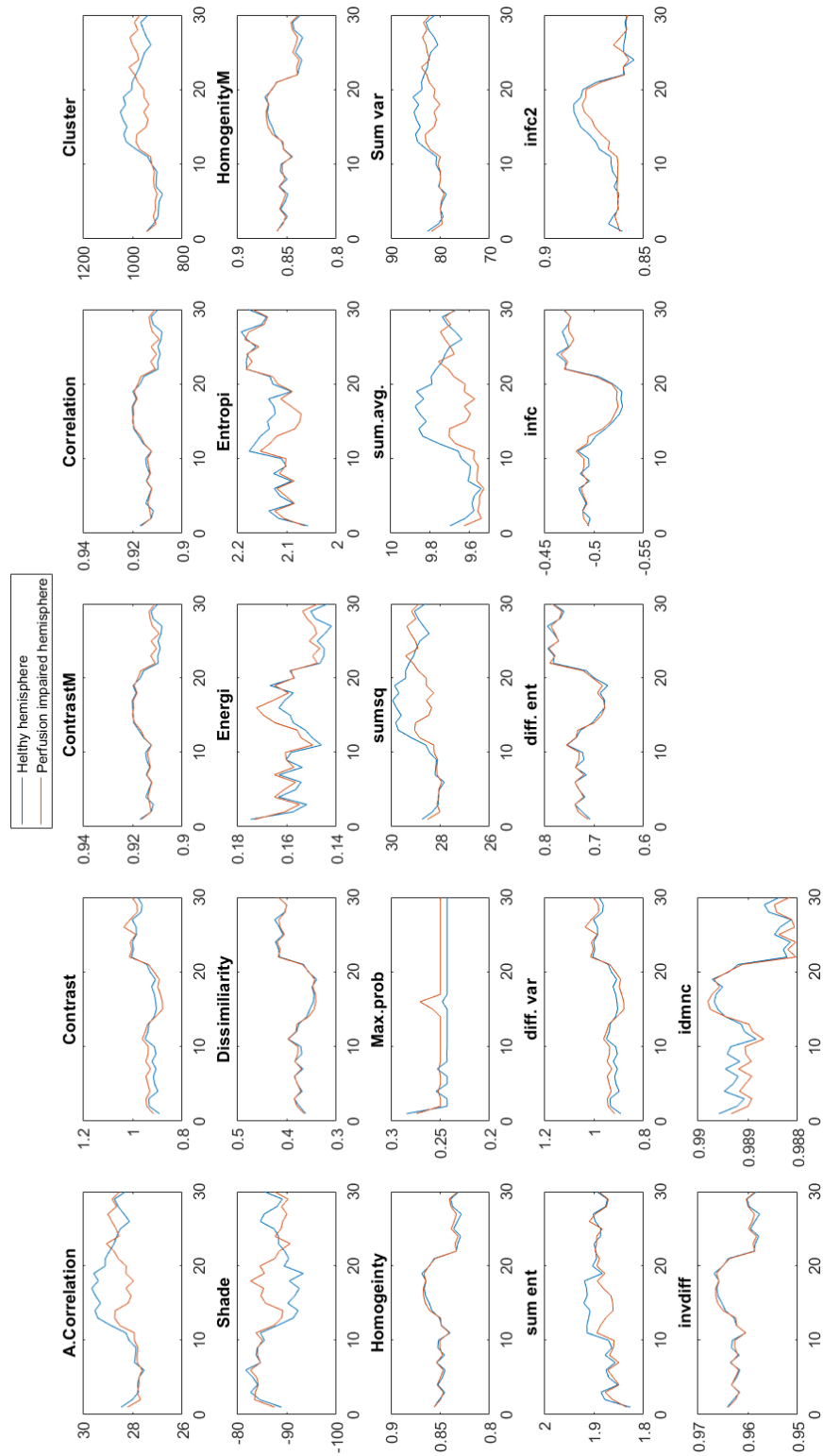
Script including all pre-processing steps.

### **regiongrowing.m**

Seeded region growing used to design binary masks [40].



# C | Features extended: GLCM



---

The features calculated and plotted above, from left to right, when read in a landscape orientation are:

- Auto-correlation
- Contrast
- Correlation: MATLAB
- Correlation
- Cluster Prominence
- Cluster Shade
- Dissimilarity
- Energy; MATLAB
- Entropy
- Maximum Probability
- Sum of Squares: Variance
- Sum Average
- Sum Variance
- Sum Entropy
- Difference variance
- Difference entropy
- Information measure of correlation1
- Information measure of correlation2
- Inverse difference Normalized (INN)
- Inverse difference moment normalized

The features can be studied closer in their corresponding reference(Haralick, 1973, [30]; Soh, 1999, [36]; Clausi, 2002, [45]).

## D | Manually Labeled Penumbra and Infarct Core

Table D.1: My caption

Patient nr.	Sum of Penumbra & Infarct core [cm <sup>2</sup> ]	Mean of Penumbra & Infarct core [cm <sup>2</sup> ]
1	398.7	30.7
2	245.3	22.3
3	177.8	16.2
4	494.5	38.1
5	485.1	37.3
6	242.9	24.3
7	311.1	28.28
8	441.4	36.7
9	376.4	20.1
10	335.9	25.8
11	536.1	44.7

## E | Additional results

This appendix includes additional results to the ones seen in chapter 5, graphs of chi-squared distance plots of  $LBP_{16,2-5}$ , wavelet (Coiflet-4) and auto-correlation extracted from the GLCMs for all 11 patients.

### Local Binary Pattern

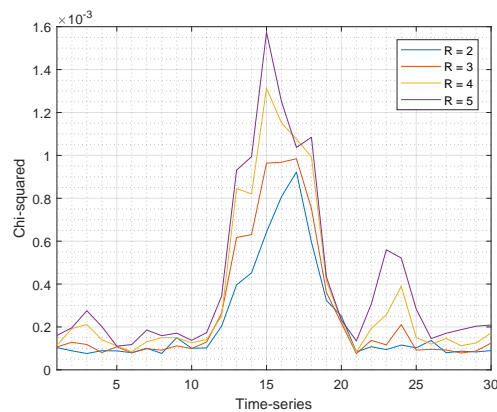


**Figure E.1:** Chi-squared distance calculated between a healthy- and a perfusion impaired hemisphere for patient 1. A LBP pattern with 16 neighbours and a radius ranging from 2-5 was used in this experiment.

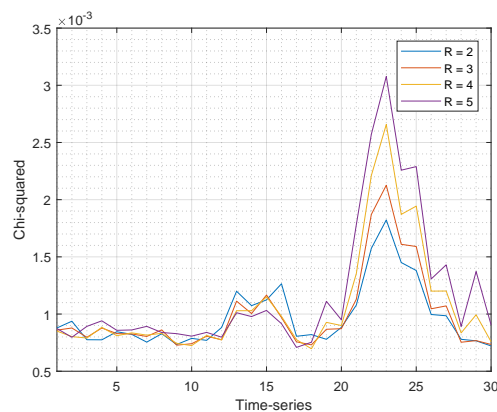


**Figure E.2:** Chi-squared distance calculated between a healthy- and a perfusion impaired hemisphere for patient 2. A LBP pattern with 16 neighbours and a radius ranging from 2-5 was used in this experiment.

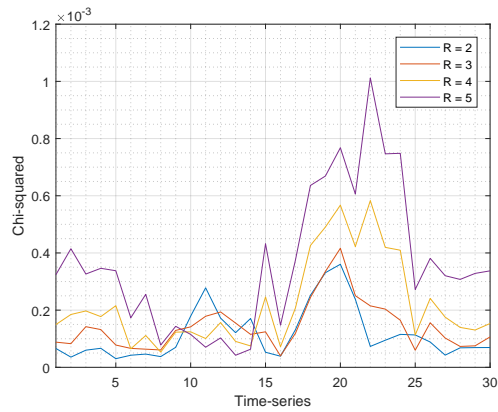


**Figure E.3:** Chi-squared distance calculated between a healthy- and a perfusion impaired hemisphere for patient 3. A LBP pattern with 16 neighbours and a radius ranging from 2-5 was used in this experiment.

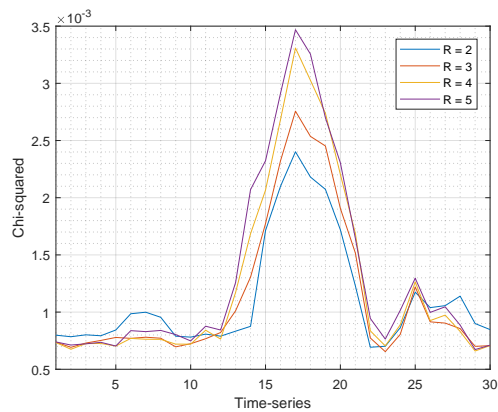


**Figure E.4:** Chi-squared distance calculated between a healthy- and a perfusion impaired hemisphere for patient 4. A LBP pattern with 16 neighbours and a radius ranging from 2-5 was used in this experiment.

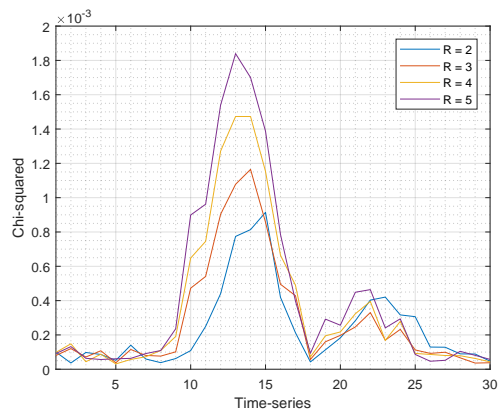


**Figure E.5:** Chi-squared distance calculated between a healthy- and a perfusion impaired hemisphere for patient 5. A LBP pattern with 16 neighbours and a radius ranging from 2-5 was used in this experiment.

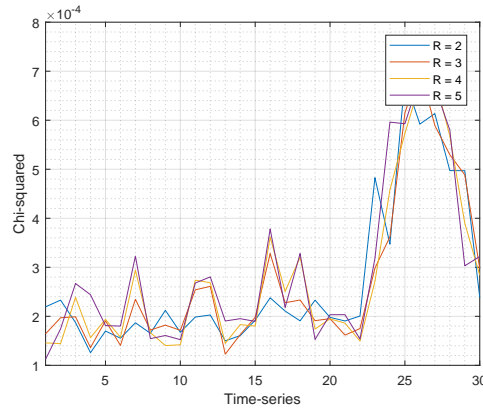


**Figure E.6:** Chi-squared distance calculated between a healthy- and a perfusion impaired hemisphere for patient 6. A LBP pattern with 16 neighbours and a radius ranging from 2-5 was used in this experiment.

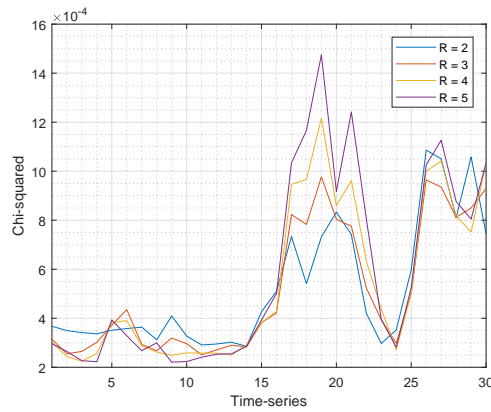


**Figure E.7:** Chi-squared distance calculated between a healthy- and a perfusion impaired hemisphere for patient 7. A LBP pattern with 16 neighbours and a radius ranging from 2-5 was used in this experiment.

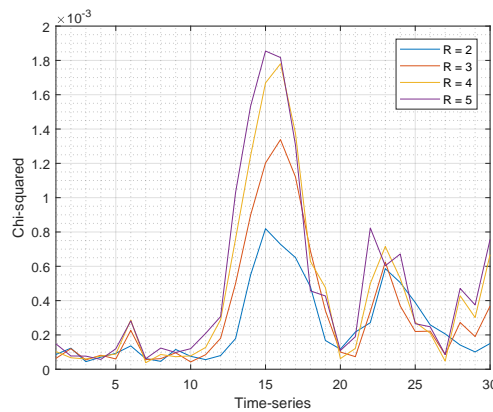


**Figure E.8:** Chi-squared distance calculated between a healthy- and a perfusion impaired hemisphere for patient 8. A LBP pattern with 16 neighbours and a radius ranging from 2-5 was used in this experiment.

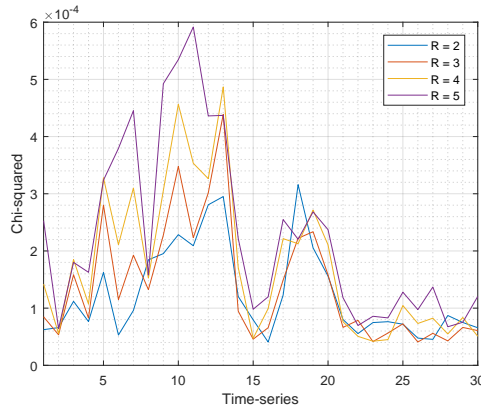


**Figure E.9:** Chi-squared distance calculated between a healthy- and a perfusion impaired hemisphere for patient 9. A LBP pattern with 16 neighbours and a radius ranging from 2-5 was used in this experiment.

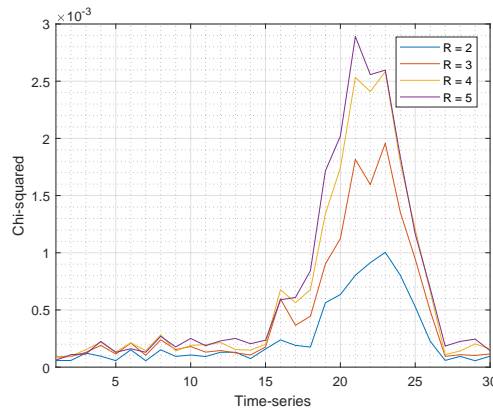


**Figure E.10:** Chi-squared distance calculated between a healthy- and a perfusion impaired hemisphere for patient 10. A LBP pattern with 16 neighbours and a radius ranging from 2-5 was used in this experiment.

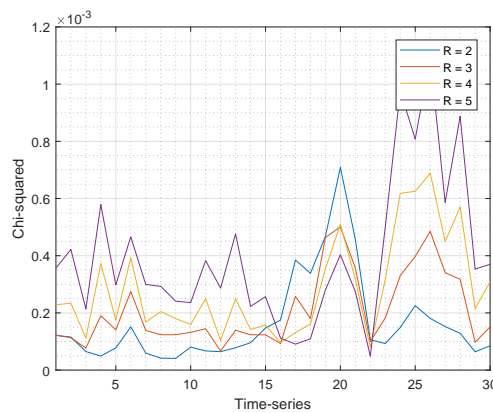


**Figure E.11:** Chi-squared distance calculated between a healthy- and a perfusion impaired hemisphere for patient 11. A LBP pattern with 16 neighbours and a radius ranging from 2-5 was used in this experiment.

---

## Wavelet

The following graphs show Chi-squared distance calculated between a healthy- and a perfusion impaired hemisphere for patient 1-4 and patient 6-11. A DWT was performed using a Coiflet-4 and a decomposition level three.

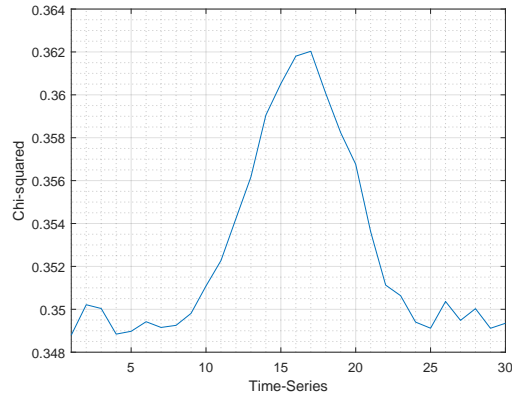


**Figure E.12:** Chi-squared distance calculated between a healthy- and a perfusion impaired hemisphere for patient 1. A DWT with the use of a Coiflet-4 and a decompositon level 3 was used in this experiment.

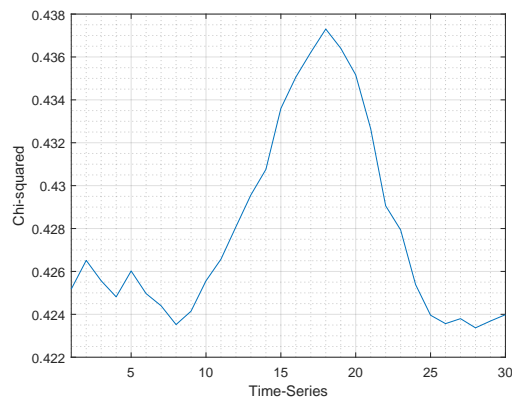


**Figure E.13:** Chi-squared distance calculated between a healthy- and a perfusion impaired hemisphere for patient 2. A DWT with the use of a Coiflet-4 and a decompositon level 3 was used in this experiment.

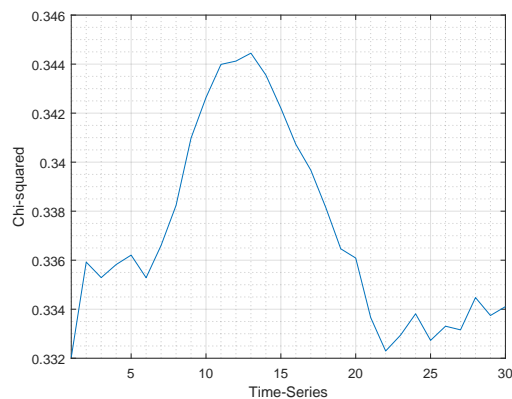


**Figure E.14:** Chi-squared distance calculated between a healthy- and a perfusion impaired hemisphere for patient 3. A DWT with the use of a Coiflet-4 and a decompositon level 3 was used in this experiment.

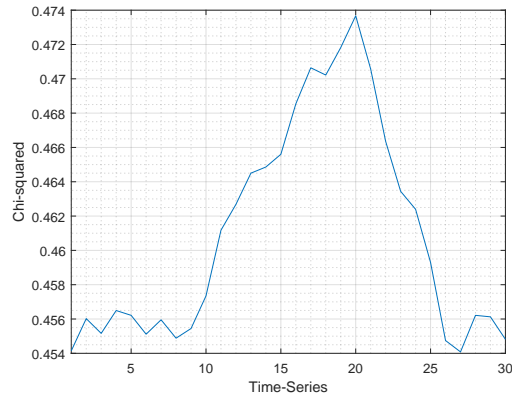


**Figure E.15:** Chi-squared distance calculated between a healthy- and a perfusion impaired hemisphere for patient 4. A DWT with the use of a Coiflet-4 and a decomposition level 3 was used in this experiment.

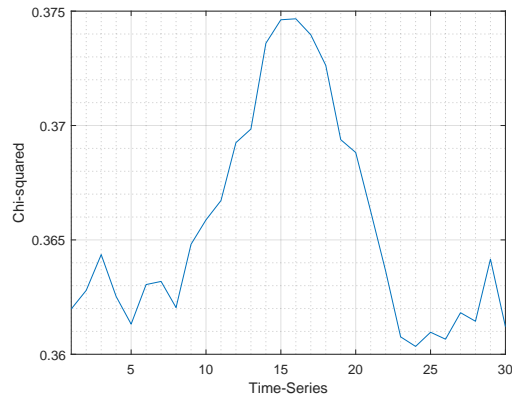


**Figure E.16:** Chi-squared distance calculated between a healthy- and a perfusion impaired hemisphere for patient 5. A DWT with the use of a Coiflet-4 and a decomposition level 3 was used in this experiment.

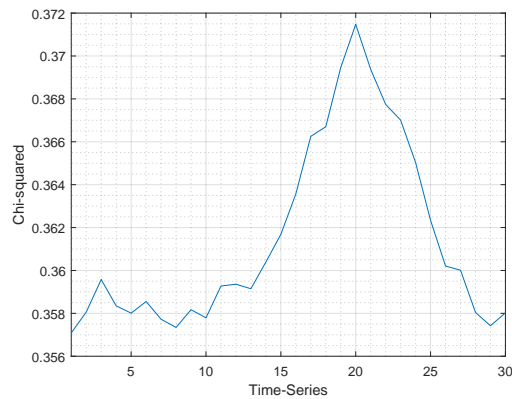


**Figure E.17:** Chi-squared distance calculated between a healthy- and a perfusion impaired hemisphere for patient 6. A DWT with the use of a Coiflet-4 and a decomposition level 3 was used in this experiment.

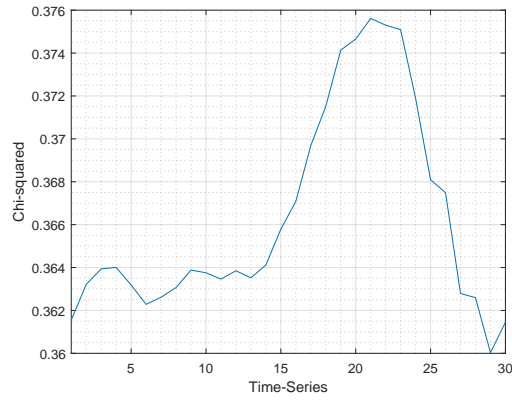


**Figure E.18:** Chi-squared distance calculated between a healthy- and a perfusion impaired hemisphere for patient 7. A DWT with the use of a Coiflet-4 and a decomposition level 3 was used in this experiment.

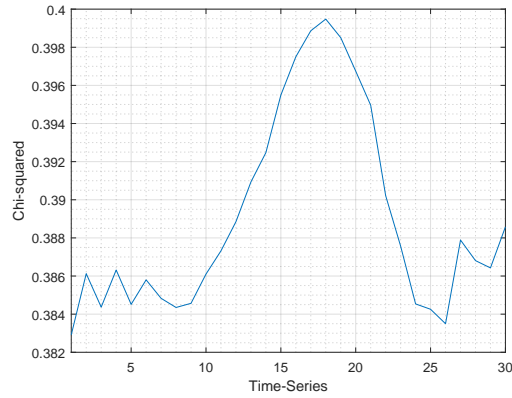


**Figure E.19:** Chi-squared distance calculated between a healthy- and a perfusion impaired hemisphere for patient 8. A DWT with the use of a Coiflet-4 and a decomposition level 3 was used in this experiment.

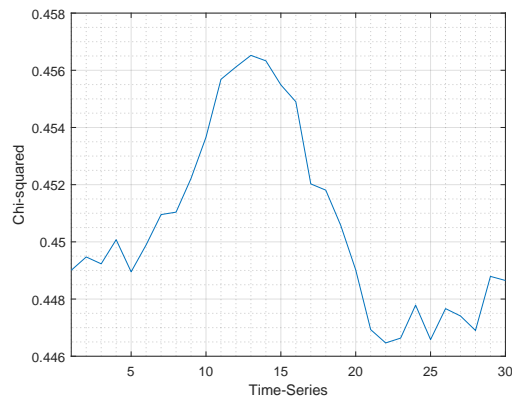


**Figure E.20:** Chi-squared distance calculated between a healthy- and a perfusion impaired hemisphere for patient 9. A DWT with the use of a Coiflet-4 and a decomposition level 3 was used in this experiment.

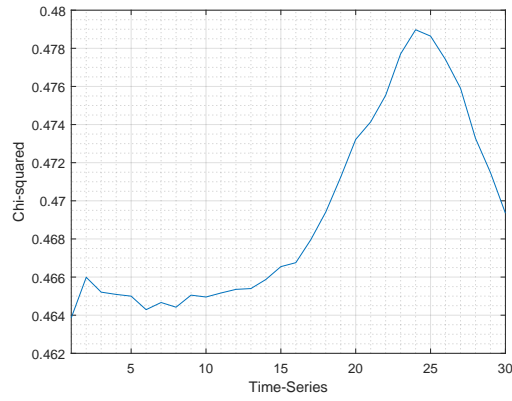


**Figure E.21:** Chi-squared distance calculated between a healthy- and a perfusion impaired hemisphere for patient 10. A DWT with the use of a Coiflet-4 and a decomposition level 3 was used in this experiment.

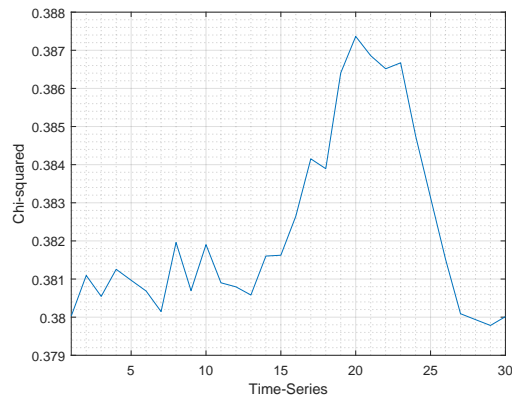


**Figure E.22:** Chi-squared distance calculated between a healthy- and a perfusion impaired hemisphere for patient 11. A DWT with the use of a Coiflet-4 and a decomposition level 3 was used in this experiment.

## Gray Level Co-occurrence Matrix

The following graphs shows auto-correlation feature extracted from GLCMs between a healthy- and a perfusion impaired hemisphere for patient 1-4 and patient 6-11.

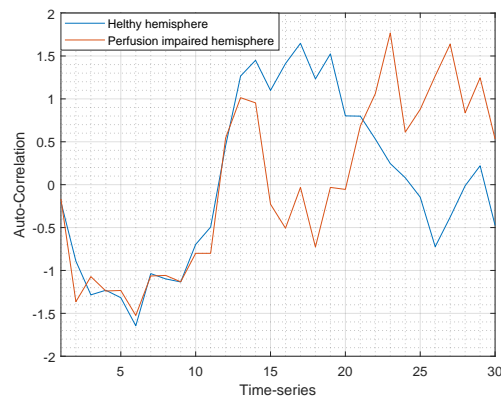


**Figure E.23:** Auto-correlation extracted from the GLCMs of patient 1 for a healthy- and a perfusion impaired hemisphere of the brain.

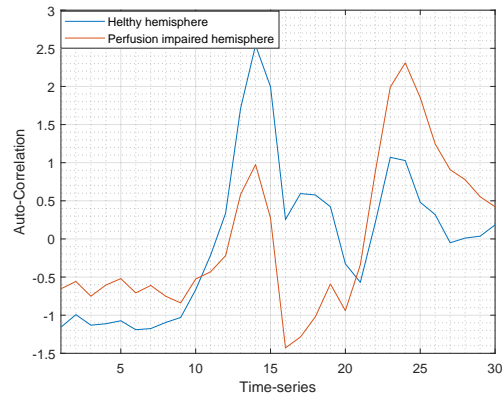


**Figure E.24:** Auto-correlation extracted from the GLCMs of patient 2 for a healthy- and a perfusion impaired hemisphere of the brain.

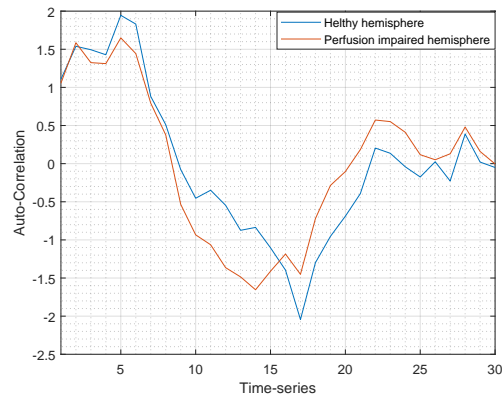


**Figure E.25:** Auto-correlation extracted from the GLCMs of patient 3 for a healthy- and a perfusion impaired hemisphere of the brain.

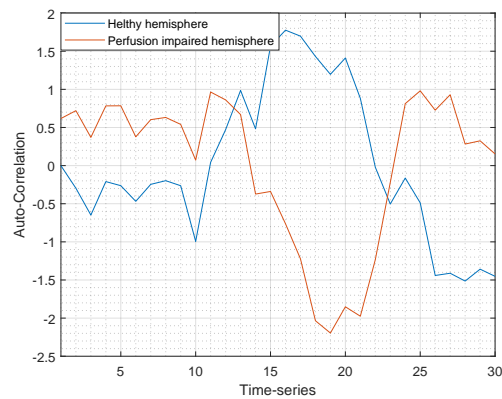


**Figure E.26:** Auto-correlation extracted from the GLCMs of patient 4 for a healthy- and a perfusion impaired hemisphere of the brain.

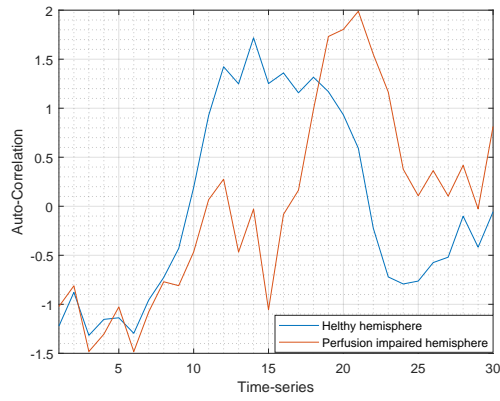


**Figure E.27:** Auto-correlation extracted from the GLCMs of patient 5 for a healthy- and a perfusion impaired hemisphere of the brain.

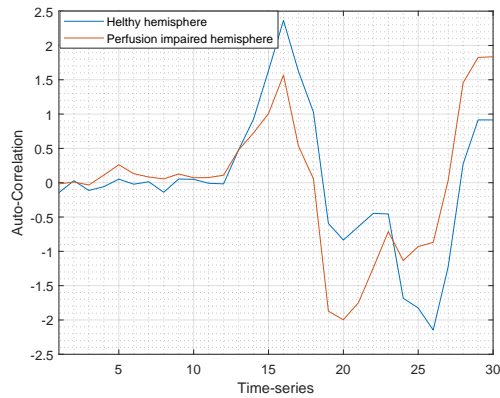


**Figure E.28:** Auto-correlation extracted from the GLCMs of patient 6 for a healthy- and a perfusion impaired hemisphere of the brain.

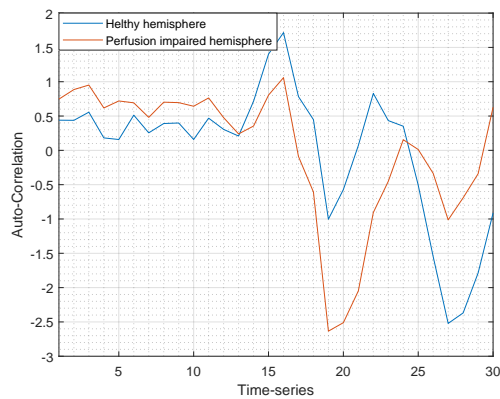


**Figure E.29:** Auto-correlation extracted from the GLCMs of patient 7 for a healthy- and a perfusion impaired hemisphere of the brain.

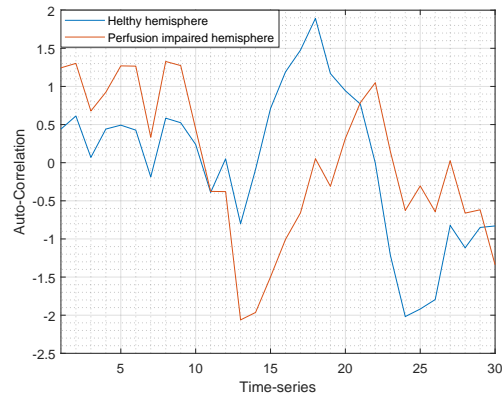


**Figure E.30:** Auto-correlation extracted from the GLCMs of patient 8 for a healthy- and a perfusion impaired hemisphere of the brain.

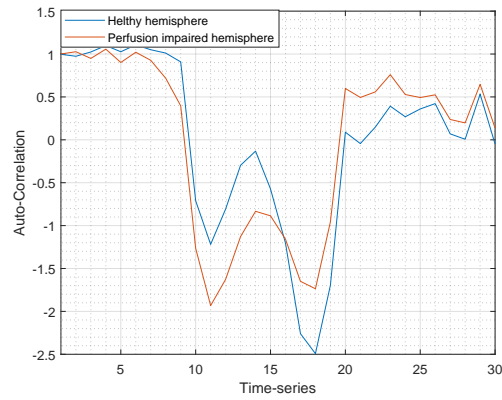


**Figure E.31:** Auto-correlation extracted from the GLCMs of patient 9 for a healthy- and a perfusion impaired hemisphere of the brain.

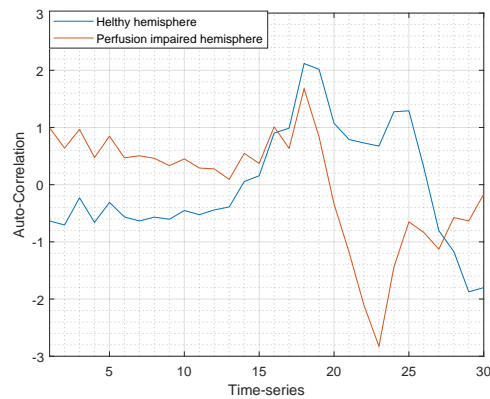


**Figure E.32:** Auto-correlation extracted from the GLCMs of patient 10 for a healthy- and a perfusion impaired hemisphere of the brain.

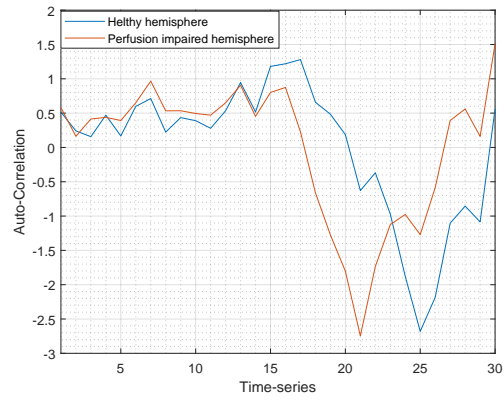


**Figure E.33:** Auto-correlation extracted from the GLCMs of patient 11 for a healthy- and a perfusion impaired hemisphere of the brain.

## F | Time-density curve

In this appendix the TDCs for all patients are available, excluded patient 5. Patient 5 is excluded as the TDC a low resolution and therefore proved hard to interpret.



**Figure F.1:** TDC for patient 1 with modified x-axis, showing time-series instead of seconds.

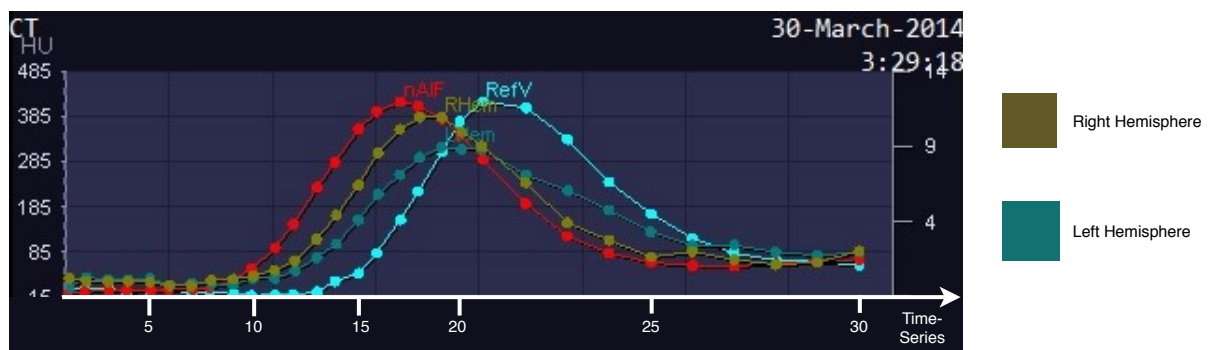


**Figure F.2:** TDC for patient 2 with modified x-axis, showing time-series instead of seconds.



**Figure F.3:** TDC for patient 3 with modified x-axis, showing time-series instead of seconds.



**Figure F.4:** TDC for patient 4 with modified x-axis, showing time-series instead of seconds.

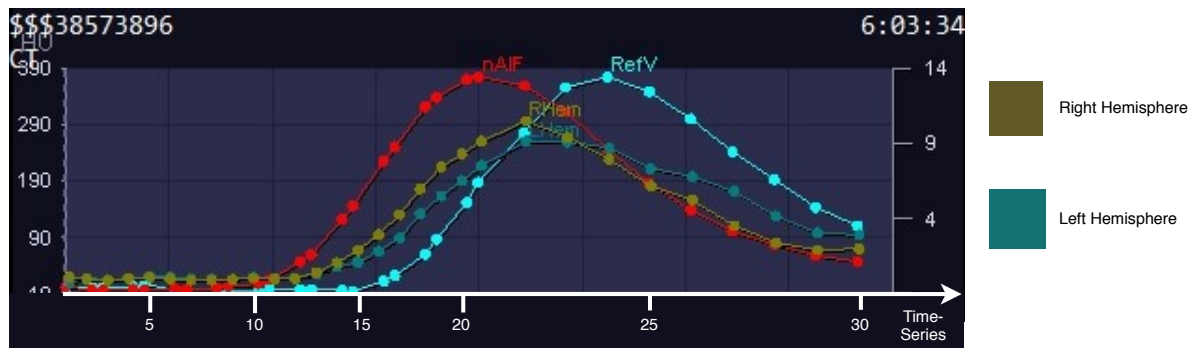


**Figure F.5:** TDC for patient 6 with modified x-axis, showing time-series instead of seconds.

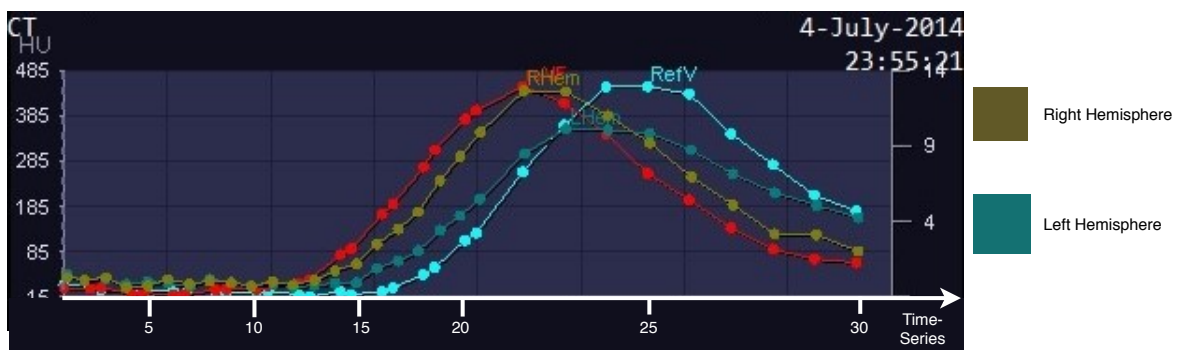


**Figure F.6:** TDC for patient 7 with modified x-axis, showing time-series instead of seconds.

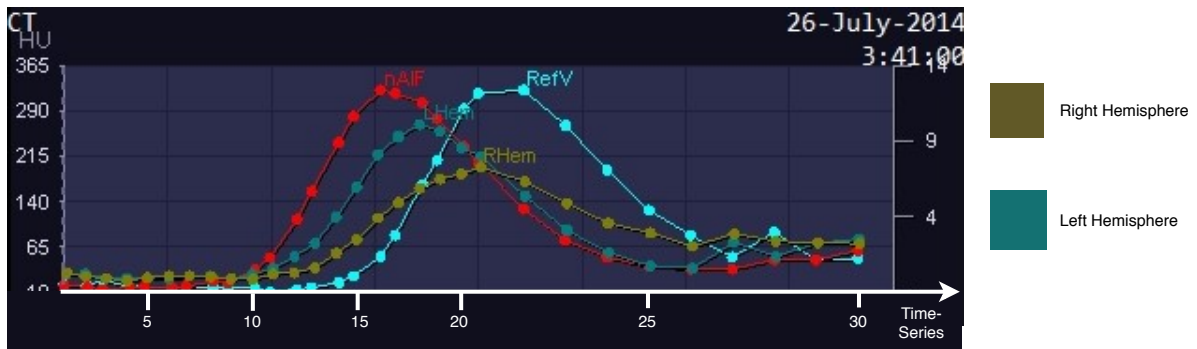


**Figure F.7:** TDC for patient 8 with modified x-axis, showing time-series instead of seconds.

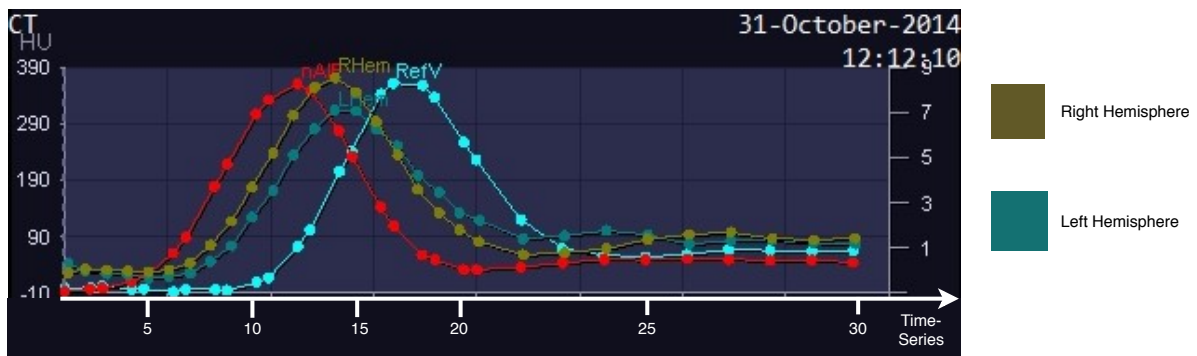


**Figure F.8:** TDC for patient 9 with modified x-axis, showing time-series instead of seconds.

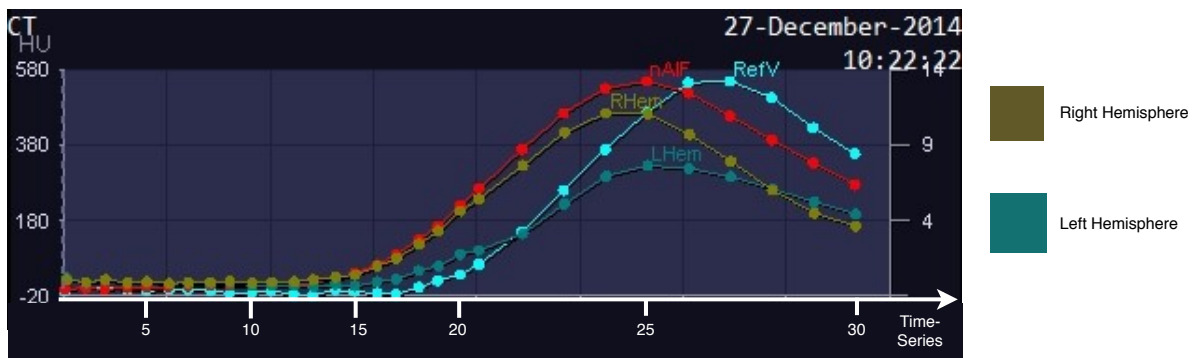


**Figure F.9:** TDC for patient 10 with modified x-axis, showing time-series instead of seconds.

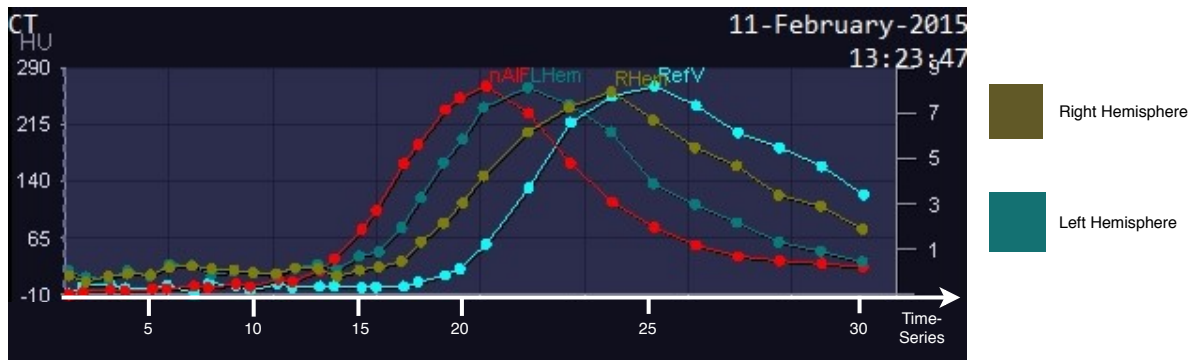


**Figure F.10:** TDC for patient 11 with modified x-axis, showing time-series instead of seconds.